Review Article

Nano Research
2022, 15(2): 818–837

ISSN 1998-0124 CN 11-5974/O4
https://doi.org/10.1007/s12274-021-3680-9

Recent progress and prospect of carbon-free single-site catalysts for the hydrogen and oxygen evolution reactions

Jingqi Guan (✉), Xue Bai, and Tianmi Tang

Institute of Physical Chemistry, College of Chemistry, Jilin University, 2519 Jiefang Road, Changchun 130021, China

Received: 13 May 2021 / **Revised:** 9 June 2021 / **Accepted**: 14 June 2021

ABSTRACT

The key challenge for scalable production of hydrogen from water lies in the rational design and preparation of high-performance and earth-abundant electrocatalysts to replace precious metal Pt and IrO_2 for hydrogen evolution reaction (HER) and oxygen evolution reaction (OER). Although atomic M-N-C materials have been extensively studied in heterogeneous catalysis field, the insufficient antioxidant capacity of carbonous substrates hinders their practical application in OER. Developing highly active and stable OER electrocatalysts is the key for electrochemical water splitting. This review presents feasible design strategies for fabricating carbon-free single-site catalysts and their applications in HER/OER and overall water splitting. The constitutive relationships between structure, composition, and catalytic performance for HER and OER are detailly discussed, providing ponderable insights into rationally constructing high-performance HER and OER electrocatalysts. The perspectives on the challenges and future research orientations in single-site catalysts for electrochemical water splitting are suggested.

KEYWORDS

single-atom catalyst, single-site catalyst, hydrogen evolution reaction, oxygen evolution reaction, water splitting

1 Introduction

As a clean energy, hydrogen gas has extensive application prospect, which can be directly used as a fuel for burning or as a cathodic reactant in fuel cells. It can also be used as an important chemical material for hydrogenation reactions. Electrochemical water splitting has been considered as a sustainable and promising method for large-scale production of H_2, using electrical energy from water power, solar energy and wind energy [1]. Water splitting is a thermodynamically uphill reaction, which includes two half-cell reactions: oxygen evolution reaction (OER) and hydrogen evolution reaction (HER) [2, 3]. It is universally known that platinum and iridium oxide are the state-of-the-art catalysts for HER and OER, respectively, nevertheless the low abundance on earth and fancy price heavily restrict their large-scale application [4–6]. Thereby, a growing body of research focuses on exploiting earth-abundant and cost-effective catalysts for HER and OER, and great achievements have been made in the past few years [7, 8]. It has been found that transition-metal sulfides, selenides, phosphides and single-site M-N-C materials can efficiently catalyze HER [9], while transition-metal oxides and hydroxides show outstanding electrochemical activity for OER in alkaline solution [10]. However, the development of noble metal-free electrocatalysts for OER in acidic media still remains a great challenge [11].

The electrocatalytic activity is mainly dependent on the geometric and electronic structure of active sites [12–15]. Numerous studies have found that the catalytic activity of metal nanoparticles significantly increases as the size of the nanoparticles decrease [16, 17]. For instance, Bard et al. investigated the correlations of the particle size of Pt and the supporting substrate with the electrochemical HER performance and found that a single Pt atom can catalyze HER [18]. Therefore, downsizing the size of the metal nanoparticles to clusters or even atomic level could afford a desired means to maximize the atom utilization and promote the electrocatalytic performance [19, 20]. In addition, for single-site catalysts, as the microenvironments of the active centers are highly uniform, the catalytic selectivity would be tremendously increased [21]. Furthermore, the catalytic mechanisms on isolated single metal sites can be well deduced by advanced characterization techniques and theoretical simulations. However, due to high surface free energy of isolated single metal atoms, they should be individually immobilized onto suitable carriers [22]. Metal oxides, hydroxides, carbides, nitrides, dichalcogenides, phosphides, and hetero-doped carbon materials can be used as substrates to support isolated metal atoms through metal-support interactions [23, 24].

In recent few years, with the improvement of synthetic strategies and characterization techniques, single-site catalysts (SSCs) or single-atom catalysts (SACs) have been extensively studied in various fields, including thermocatalytic reactions [25]. organic catalytic reactions [26], photocatalytic reactions [27], electrocatalytic reactions [28], and biocatalytic reactions [29]. With the help of aberration-corrected scanning transmission electron microscopy (AC-STEM), X-ray absorption spectroscopy (XAS) and density functional theory (DFT) simulations, the application of single-site catalysts in electrocatalytic water splitting has been rapidly developed. In 2015, Tour and co-workers found that atomic cobalt embedded into nitrogen-doped graphene exhibited excellent HER activity in acidic and alkaline media [30]. In 2018, Huang et al. found that atomically dispersed

Address correspondence to guanjq@jlu.edu.cn

Ni embedded into nitrogen-doped graphene with NiN_4C_4 configuration exhibited excellent OER activity in alkaline media [31]. Guan et al. found that MnN_4 moiety embedded into nitrogen-doped graphene exhibited outstanding chemical and electrochemical water oxidation [32]. These findings are significant breakthroughs to construct single metal active sites for electrocatalytic HER and OER.

Much of the previous research focused on carbon-based single-site catalysts (especially M-N-C materials) for electrocatalytic HER and OER due to good electrical conductivity of carbon-based substrates [33, 34]. However, carbon-based materials are unstable and would be oxidized under oxidizing conditions [35]. Besides, the anchored single metal atoms would be leached by oxidizing and breaking the chemical bonds between metal ions and ligands in the support, which would lead to the deactivation. Therefore, it is attractive to develop carbon-free single-site catalysts for electrochemical water splitting. In this review, we provide a summary on carbon-free single-site catalysts for electrochemical HER/OER and overall water splitting. Firstly, we will systematically introduce how to fabricate isolated single metal sites onto carbon-free supports. Secondly, we will illustrate how to identify the atomic structures of isolated single metal sites. Thirdly, we will emphasize the applications of carbon-free single-site catalysts for electrochemical HER/ OER and overall water splitting by analyzing specific cases. Finally, we will put forward the challenges and personal perspectives of the future developments of carbon-free single-site catalysts for electrocatalytic water splitting.

2 Synthesis and characterization of carbon-free single-site catalysts

2.1 Synthetic methods

2.1.1 *Wet chemistry*

Due to high surface energy and unsaturated coordination environment, single-site metal species are in a metastable state, which squint towards agglomeration into clusters or nanoparticles [23]. For the preparation of high-quality single-site catalysts, it is crucial to immobilize the metal species and geographically isolate metal ions from touching each other during synthetic procedure. It is preferential to choose substrates with high specific surface area and abundant O/S/N-containing functional groups to anchor isolated metal species and prevent their agglomeration after post-treatment.

Wet chemistry methods are those that operate in solution, which include impregnation method, chemical reduction, and so on. Propitious fabrication of single-site catalysts based on wet chemical methods usually requires: (i) low metal loading content to prevent the reunion and make sure atomic dispersion of metal species; (ii) suitable support with abundant O-containing functional groups that can disperse well in the solution and coordinate with metal ions to generate strong metal-support interactions. Two key steps are involved in wet chemistry methods: (i) the metal species are supported on the substrate, which are further separated from the solution; (ii) the metal-support interactions are enhanced and the electronic structure of isolated metal sites is modulated by calcination or reduction.

Song et al. incorporated highly dispersed Ir (including single atoms and clusters) onto $Co(OH)_2$ nanosheets by simple chemical reduction of Co^{2+} and Ir^{4+} with sodium borohydride in water solution [36]. Gu and co-workers synthesized $IrCoO_x$ by reduction of Co^{2+} and Ir^{4+} with sodium borohydride in water solution containing cetyltrimethylammonium bromide [37]. After annealing at 450 °C in air for 2 h, atomically dispersed Ir were embedded in the framework of amorphous CoO_x. Moreover, they also incorporated isolated Ni atoms into the framework of MoS_2 by immersing $NiCl_2$ onto the MoS_2/CC (Ni_{SA}-MoS_2/CC) and subsequent annealing at 300 °C under the 10% H_2/Ar atmosphere [38]. From the high-angle annular dark-field scanning transmission electron microscopy (HAADF-STEM) image and corresponding electron energy loss spectroscopy (EELS) spectra (Figs. 1(a)–1(e)), the single Ni atom located at the H-basal site and in the S-edge. Cao et al. anchored atomic Ru onto MoS_2 nanosheets by a simple impregnation method as shown in Fig. 1(f) [39]. The mass loading of Ru can reach ca. 3.1%.

Although wet chemistry methods are easily operated and can be adopt for mass preparation of catalysts, it is very challenging to obtain high-quality single-site catalysts with high metal loading density. Metal clusters and nanoparticles are inevitably formed during the synthetic process and/or post-treatment when the metal loading is relatively high. In addition, without high temperature treatment, the anchored metal atoms are hardly incorporated into the lattice of substrates, which is detrimental for their durability during catalytic reactions.

2.1.2 *Hydrothermal synthesis*

Hydrothermal synthesis is performed in aqueous solution at 100–1,000 °C under the pressure of 1 MPa–1 GPa. Under subcritical and supercritical hydrothermal conditions, the reactivity of the reaction is greatly enhanced because the reaction is at the molecular level. Therefore, the hydrothermal reaction

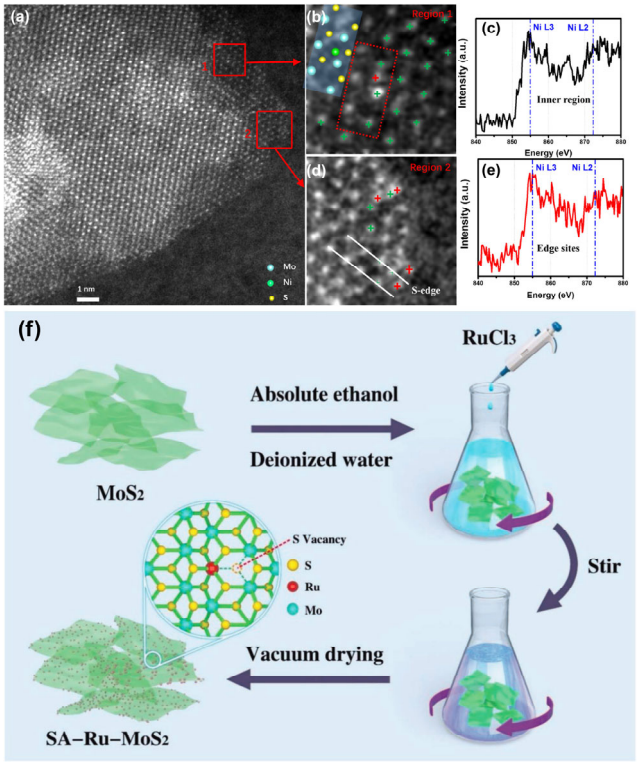

Figure 1 (a) HAADF-STEM images of Ni_{SA}-MoS_2/CC and corresponding higher-magnification views of (b) region 1 and (d) region 2 (Ni atoms: red cross, Mo atoms: green cross). Corresponding Ni EELS spectra of (c) inner region 1 and (e) edge sites at region 2. (f) Synthetic illustration of the SA-Ru-MoS_2. (a)–(e) Reproduced with permission from Ref. [38], © Elsevier Ltd. 2018. (f) Reproduced with permission from Ref. [39], © WILEY-VCH Verlag GmbH & Co. KGaA, Weinheim2019.

can replace some high temperature solid reactions. In the hydrothermal synthesis system, different synthesis routes have been developed, such as direct method, seed method, guide agent method, template method, complexing agent method, organic solvent method, microwave method, and high-temperature and high-pressure synthesis technology. In water solution, it is nominated as hydrothermal synthesis, while in organic solvent, it is denoted as solvothermal synthesis.

Deng and co-workers doped atomic Rh at the in-plane S sites of MoS_2 with 3–6 layers using a solvothermal reaction [40]. A mixture of $(NH_4)_6Mo_7O_{24}{\cdot}4H_2O$, $(NH_4)_3RhCl_6$, and CS_2 was allowed to react in water solution under Ar protection at 400 °C for 4 h to obtain atomic Rh doped MoS_2. From the HAADF-STEM image and corresponding TEM simulations, the atomic Rh were successfully incorporated into the lattice substituting the Mo atoms of 2H-MoS_2 (Fig. 2). Moreover, the average inter-Rh distances can be regulated by adjusting the doping content of Rh. Tsang et al. doped four different transition metals (Fe, Co, Ni and Ag) onto MoS_2 by a hydrothermal method [41]. They used MoS_2 nanosheets as the precursor and different metal ions and thiourea as the dopant and S-source, respectively. After hydrothermal reaction at 160 °C for 24 h, the metal dopants can be successfully incorporated on the surface of MoS_2.

2.1.3 *Chemical vapor deposition*

Chemical vapor deposition (CVD) is a process in which substances in the gaseous or vapor state react on the gas phase or the gas-solid interface to form solid sediments. Three main stages are involved in the CVD process: (i) reaction gas diffuses to the substrate surface, (ii) the reaction gas is adsorbed to the substrate surface, (iii) chemical reaction takes place to produce solid sediments, and the gas by-products are separated. The chemical reaction in atomic layer deposition (ALD) is like that in CVD, but the requirements of deposition conditions and the quality of deposition layer in ALD are different from traditional CVD. Thin-film materials can be synthesized by CVD or ALD techniques.

Wei and co-workers synthesized Co-MoS_2 flakes with homogeneously dispersed Co by CVD method [42]. They used Co-doped MoO_3 and S powder as the precursors. The sulfur gas will react with Co-MoO_3 gas on the SiO_2/Si substrates

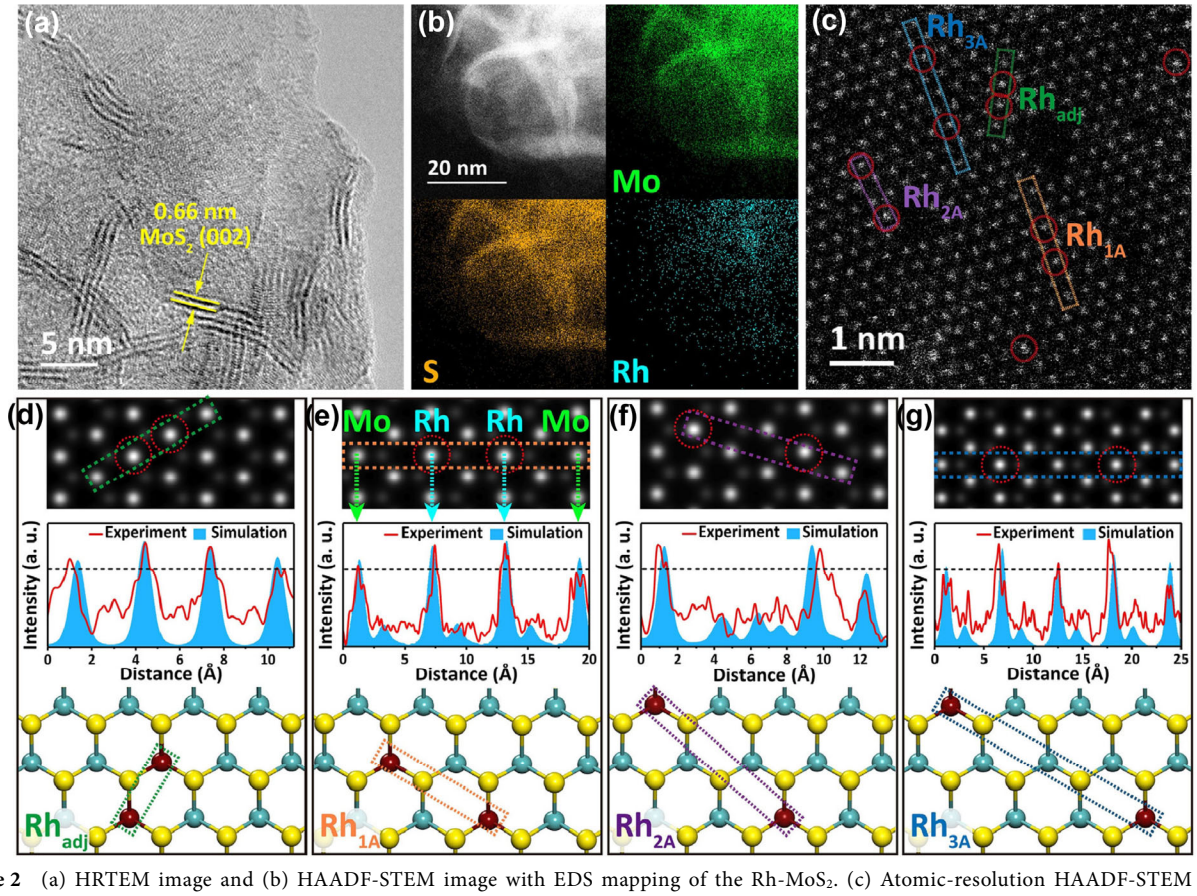

Figure 2 (a) HRTEM image and (b) HAADF-STEM image with EDS mapping of the Rh-MoS_2. (c) Atomic-resolution HAADF-STEM image. (d)–(g) Corresponding TEM simulations, linear intensity profiles, and illustrations of the Rh_{adj}, Rh_{1A}, Rh_{2A}, and Rh_{3A} structures, respectively, in (c). S yellow, Mo cyan, Rh brown spheres. (a)–(g) Reproduced with permission from Ref. [40], ©WILEY-VCH Verlag GmbH & Co. KGaA, Weinheim 2020.

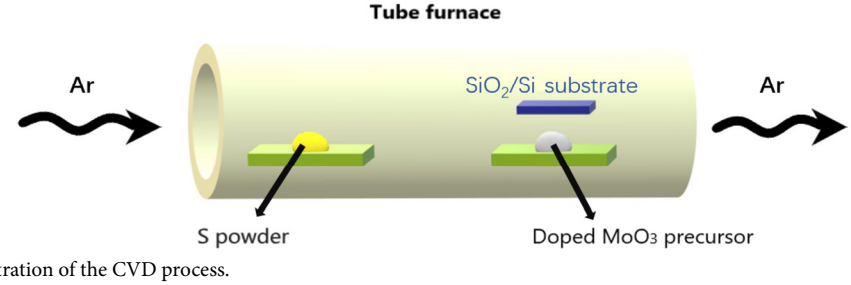

Figure 3 Schematic illustration of the CVD process.

at 850 °C to form Co-MoS_2 as shown in Fig. 3. Lin et al. anchored atomic Pt onto a porous NiO by ALD technique [43]. They used $MeCpPtMe_3$ as the Pt source and O_3 as the oxidant, which were allowed to react on the surface of NiO at 240 °C for Pt deposition. For CVD or ALD, isolated metal species are usually supported on the surface and pores of the substrate. Therefore, the substrate should possess high specific surface area or porous structure for high dispersion of supported metal species. Since specialized equipment is needed, it is hard to prepare single-site catalysts on a large scale.

2.2 Identification of the structure of isolated single metal sites

The analysis of atomic configurations of active sites is crucial for acquiring structure-property-performance relationships of SACs in electrocatalytic reactions, which can be employed to direct further designs of high-performance electrocatalysts. The doped single metal atoms can be directly observed by advanced aberration-corrected scanning transmission electron microscopy (AC-STEM). However, if the atomic number of the doped metal is close to that of the substrate or two different transition metal elements are co-doped onto a support, it is very hard to distinguish them. In this case, the corresponding cross-sectional intensity of selected area in the HAADF-STEM with aberration correction can afford the atom contrast [42, 44]. Moreover, the EELS or energy dispersive spectrometer (EDS) coupled with the STEM can provide the dispersion of various elements in single-site catalysts. Additionally, the isolated single metal atoms on metal oxide supports can be identified by atomic resolution spectrum of STEM-EELS or STEM-EDX. For instance, Zelenay and co-workers used EELS spectra to clearly identify that isolated single Fe atoms were adjacent to N atoms [45]. However, a longer time is required to acquire the data than STEM imaging. Therefore, for STEM-EELS and STEM-EDX measurements, the voltage of electron beam should be lowered to reduce the beam intensity. Although isolated single metal atoms can be observed by HAADF-STEM, the chemical valence of metal ions cannot be determined due to weak signal and instability of metal atoms under the electron beam.

The oxidation state of metal species can be characterized by X-ray photoelectron spectroscopy (XPS), electron paramagnetic resonance (EPR), and X-ray absorption near edge structure (XANES). Thereinto, XPS is a near-surface sensing technology, which affords quantitative or qualitative information on the chemical bonding of metal and nonmetal atoms within near-surface regions [46]. The change in the chemical valence and local chemical surroundings can be reflected by the chemical shift of electron binding energy. The surface content of various elements can be calculated based on the intensity of the peaks. However, the fine structure of isolated metal atoms cannot be well disclosed by XPS. To better understand the coordination environment (including coordination number and bond length) of isolated metal sites, extended X-ray absorption fine structure (EXAFS) is generally adopted. Combining the EXAFS characterization results with theoretical simulations, the local structure of isolated metal sites can be obtained. For example, Zheng and co-workers found Co-S covalent bond with bond length of 0.2384 nm and coordination number of 3.8 in atomic cobalt doped 1T MoS_2 by EXAFS [47]. To monitor the dynamic process in electrocatalytic reactions, *in situ* technologies (especially *Operando* X-ray absorption spectroscopy) can be used to detect the structural change of active sites and uncover reaction mechanisms.

3 Catalytic mechanisms for hydrogen and oxygen evolution reactions

The electrochemical HER has been widely investigated and the reaction mechanism has been well established [48]. Two kinds of reaction mechanisms were widely known for HER in acidic or alkaline media (Fig. 4(a)) [1, 48–50]. One is Volmer-Tafel mechanism, where the H_3O^+ or H_2O are dissociated on the catalyst surface to generate absorbed hydrogen species (H_{ads}) (Eqs. (1) and (3)). After high coverage of H_{ads} on the surface, two contiguous H_{ads} species combine to form H_2 (Eqs. (2) and (4)). The other well-known mechanism for HER is Volmer-Heyrovsky mechanism, where the initial step is the same with that in Volmer-Tafel mechanism (Eqs. (5) and (7)). Due to low coverage of H_{ads} on the catalyst surface, the distance between two neighboring H_{ads} is too far away to bond together and they would couple with an electron and a proton to produce H_2 (Eqs. (6) and (8)).

(i) Volmer-Tafel reaction mechanism in acidic media (H_{ads} indicates adsorbed intermediate)

$$H_3O^+ + e^- \rightarrow H_{ads} + H_2O \quad (1)$$

$$2H_{ads} \rightarrow H_2 \quad (2)$$

In alkaline media:

$$H_2O + e^- \rightarrow H_{ads} + OH^- \quad (3)$$

$$2H_{ads} \rightarrow H_2 \quad (4)$$

(ii) Volmer-Heyrovsky reaction mechanism in acidic media:

$$H_3O^+ + e^- \rightarrow H_{ads} + H_2O \quad (5)$$

$$H_{ads} + H_3O^+ + e^- \rightarrow H_2 + H_2O \quad (6)$$

In alkaline media:

$$H_2O + e^- \rightarrow H_{ads} + OH^- \quad (7)$$

$$H_{ads} + H_2O + e^- \rightarrow H_2 + OH^- \quad (8)$$

The rate-limiting step of HER is generally determined by the bonding strength of adsorbed H* on the active sites. If the bonding strength is too weak, the HER is controlled by the adsorption process (Volmer step), while the bonding strength is too strong, the desorption step (either the Heyrovsky step or the Tafel step) will dominate the reaction [50]. Therefore, a desired HER electrocatalyst should possess moderate bonding strength with adsorbed H*, which favors the formation of H_2. The Tafel slopes in Volmer–Tafel and Volmer–Heyrovsky mechanism are typically determined as 29 and 38 $mV \cdot dec^{-1}$, respectively. From the diagram by plotting exchange current density against the H adsorption free energy (ΔG_{H^*}) (Fig. 4(b)) [51], Pt is located at the apex of the volcano with $\Delta G_{H^*} = 0$, indicating the highest HER activity.

The OER involves several electron/proton transfers, which can operate in either acidic ($2H_2O \rightarrow O_2 + 4H^+ + 4e^-$) or alkaline ($4OH^- \rightarrow O_2 + 2H_2O + 4e^-$) media as illustrated in Fig. 4(c) [52]. In acidic media, two water molecules are oxidized to generate one O_2 molecule with four proton-coupled electron transfer steps (Eqs. (9)–(12)). In alkaline media, four hydroxyl groups are transformed into one O_2 molecule and two water molecules with four electron transfer steps (Eqs. (13)–(16)).

In acidic media (*denotes the active site, and OH*, O*, and OOH* indicate adsorbed intermediates):

$$H_2O + * \rightarrow OH^* + H^+ + e^- \quad (9)$$

$$OH^* \rightarrow O^* + H^+ + e^- \quad (10)$$

$$O^* + H_2O \rightarrow OOH^* + H^+ + e^- \quad (11)$$

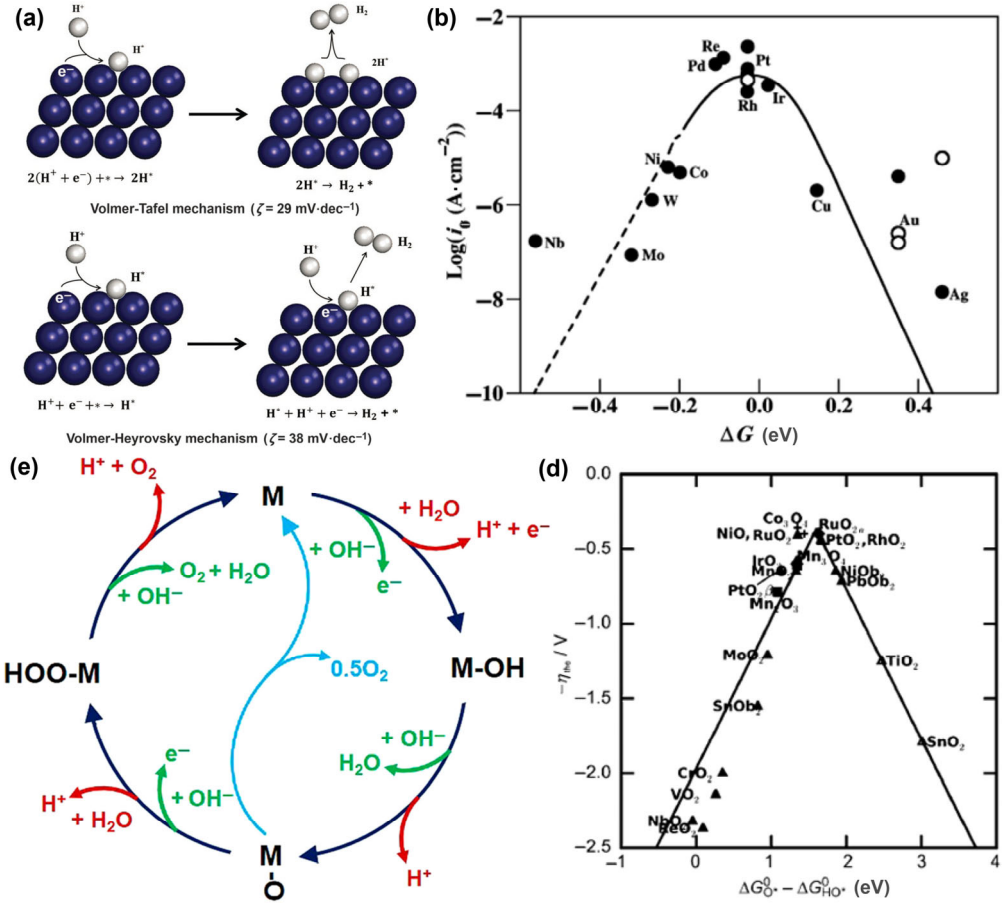

Figure 4 (a) HER mechanisms on the catalyst surface. (b) The volcano plot for HER. (c) OER mechanism for alkaline (red route) and acidic (green route) conditions. (d) Activity trends for various oxides for OER. (a) Reproduced with permission from Ref. [1], © WILEY-VCH Verlag GmbH & Co. KGaA, Weinheim 2019. (b) Reproduced with permission from Ref. [51], © American Chemical Society 2010. (c) Reproduced with permission from Ref. [52], © American Chemical Society 2018. (d) Reproduced with permission from Ref. [53], © Wiley-VCH Verlag GmbH & Co. KGaA, Weinheim 2011.

$$OOH^* \rightarrow * + O_2 + H^+ + e^- \quad (12)$$

In alkaline media:

$$OH^- + * \rightarrow OH^* + e^- \quad (13)$$

$$OH^* + OH^- \rightarrow O^* + H_2O + e^- \quad (14)$$

$$O^* + OH^- \rightarrow OOH^* + e^- \quad (15)$$

$$OOH^* + OH^- \rightarrow * + O_2 + H_2O + e^- \quad (16)$$

The OER mechanism can be roughly estimated by the measured Tafel slope, which can reflect the electron transfer coefficient. Generally, the smaller Tafel slope is, the more efficient OER kinetics is. According to the classical Butler–Volmer formalism, a slope near 24 mV·dec^{-1} indicates that the third electron transfer is the potential-determining step, while a Tafel slope near 40 mV·dec^{-1} indicates that the second electron transfer is the potential-determining step [54]. A Tafel slope near 60 mV·dec^{-1} indicates that the potential-determining step is followed the first electron transfer. However, it should be noted that the real OER on heterogeneous catalysts might be very complicated, and the OER process depends consumingly on the structure of active sites, which might not simply follow the Butler–Volmer mechanistic kinetics. Rossmeis et al. plotted OER overpotential (η^{OER}) as function of $\Delta G^0_{O^*} - \Delta G^0_{HO^*}$ for estimating the activity of various oxides and found that the activity tendency follows: $Co_3O_4 \approx RuO_2 > PtO_2 \approx$ rutile phase $\approx RhO_2 > IrO_2 \approx Mn_xO_y \approx NiOb_2 \approx RuO_2$ and IrO_2 anatase phase > $PbOb_2$ >> Ti, Sn, Mo, V, Nb, and Re oxides (Fig. 4(d)) [53].

To deeply understand the reaction mechanism, *in situ* or operando spectroscopic technologies have been developed to monitor the chemical speciation on surface active sites during the OER. For example, Nilsson and co-workers used synchrotron-radiation-based ambient-pressure photoelectron spectroscopy (APXPS) to *in situ* observe surface species on IrO_2 nanoparticles during the OER (Fig. 5(a)) [55]. They found that both iridium-based oxide and hydroxide species coexisted after IrO_2 nanoparticles touched water and the hydroxide will be transformed into oxide during electrocatalytic process. The OER on IrO_2 was a potential-dependent change through a deprotonation mechanism, where Ir^{IV} was oxidized to Ir^{V}, a key species for the reaction. Jones et al. developed *in situ* X-ray photoemission and absorption spectroscopy to detect surface species of iridium-based catalysts during the OER (Fig. 5(b)) [56]. They found that the electrophilic O^{I-} species in the IrO_2 should be responsible for the O–O bond formation:

$$IrO_xO^{I-} + H_2O \rightarrow IrO_xO^{I-}\text{–}O^{I-}\text{–}H + H^+ + e^- \rightarrow IrO_x + O_2 + 2H^+ + 3e^- \quad (17)$$

Minguzzi et al. investigated the change of the oxidation states of iridium species during OER by *in situ* XAS and found that Ir^{III} and Ir^{V} co-existed at the onset potential [57]. According to the *in situ* results, they proposed a fast cycling of the Ir^{V}/Ir^{III} couple during the electrocatalytic OER. In addition, *in situ* XAS technique can not only detect the change of oxidation states of active species during electrocatalysis, but also monitor the structural change of active sites. For example, Hu et al. used *Operando* XAS technique to monitor the structural change of

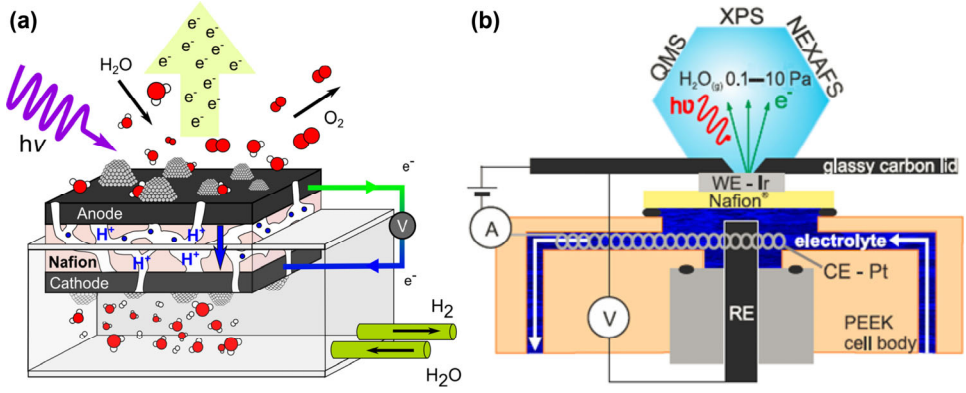

Figure 5 (a) Schematic drawing of a PEM electrochemical cell setup for APXPS investigations. (b) Three-electrode *in situ* cell for XPS and NEXAFS measurements. (a) Reproduced with permission from Ref. [55], © WILEY-VCH Verlag GmbH & Co. KGaA, Weinheim 2014. (b) Reproduced with permission from Ref. [56], © The Royal Society of Chemistry 2017.

active sites in a single-atom Co-N-C precatalyst during OER and found that the CoN_3C_1 site will be transformed into a more active Co-Fe-N-C site with the addition of Fe^{3+} ions [58]. Therefore, they proposed a dimeric Co-Fe structural motif as the active site for the OER.

Due to low concentration of reaction intermediates on the active sites and their very short life, they can hardly be detected by experimental detection. Therefore, we need theoretical calculations (DFT and other theoretical methods) to simulate reasonable reaction routes and predict possible reaction intermediates during the electrocatalytic HER/OER [59]. For HER, the reaction rate is mainly determined by the ΔG_{H^*}. If the binding between hydrogen and the active site is too weak, the adsorption (Volmer) step is the rate-determining step, while if hydrogen binds to the active site is too strongly, the desorption (Heyrovsky/Tafel) step will be the potential-determining step [60]. For OER, the binding energies of key intermediates including *O, *OH and *OOH on active sites strongly affect the electrocatalytic activity [61]. Therefore, it is crucial to correlate the binding energies with the electronic structure of single-site catalysts [59].

4 Applications of single-site catalysts

4.1 HER performance

4.1.1 Single metal atoms doped transition metal dichalcogenides for HER

MoS_2 has a typical sandwich-layered structure, where a hexagonal plane of molybdenum atoms is wedged between two other hexagonal planes of sulphur atoms via strong covalent bonding [41]. Neighboring layers are settled by weak van der Waals forces. The inert basal plane of MX_2 (M = Mo, W, or V; X = S or Se) seriously restricts the electrocatalytic activity owing to poor electronic transfer property, resulting in sluggish kinetics. For HER, Mo edges (1010) and S edges (1010) afford the active centers. By real-time surface-enhanced Raman spectroscopy (SERS), Zhang and co-workers identified that the S atoms of single layer MoS_2 are the active center for electrocatalytic HER [62]. Two-dimensional MoS_2 exhibits higher HER activity than bulk MoS_2 owing to more exposed active sites. To create more active sites on the basal plane of MoS_2, defect engineering and single-atom doping strategy are preferentially adopted [63].

Single cobalt atom can be immobilized into single-layered MoS_2 by different methods, including hydrothermal method [41], electrochemical leaching method [47], and CVD method [42]. By lithium intercalation, Tsang et al. exfoliated bulk MoS_2 precursor to obtain monolayer MoS_2 nanosheets [41]. Then, they doped atomic Fe, Co, Ni and Ag onto the MoS_2 nanosheets by a hydrothermal reaction and found that single-atom Co doped MoS_2 exhibited the best HER performance (Figs. 6(a)–6(c)). The doped Co atoms would interact with S atoms, lowering ΔG_{H^*} and increasing HER activity. Moreover, the doped Ni atoms would interact with Mo atoms, increasing $|\Delta G_{H^*}|$ and thus decreasing HER activity. Cui et al. found that the 2H phase of MoS_2 would be transformed to D-1T phase by lattice strain and Co-S interaction, leading to improved HER activity [47]. Wei et al. doped isolated Co atoms into monolayer MoS_2 to form a long-range ferromagnetic order and found that the Co-S interaction can enhance the electronic density of S atoms, thus improving the H adsorption ability of basal plane S sites (Figs. 6(d)–6(l)) [42]. Yao et al. found that the electronic state density of S atoms coordinated with Co atoms would decrease compared with that of S atoms in basal planes, leading to enhanced hydrogen adsorption on the Co-S site and small $|\Delta G_{H^*}|$ for HER [64].

In addition to single Co atoms, isolated Ni atoms can also modulate the basal plane of MoS_2 nanosheets and coordinate with S atoms to adjust their electronic states, thus optimizing the adsorption energy of H atoms and boosting HER activity. By impregnation method, Lou et al. obtained single-atom Ni decorated MoS_2 nanosheets, which exhibited higher HER activity than pristine MoS_2 [65]. Moreover, Gu and co-workers found that the isolated Ni atoms were mainly located at S-edge sites and H-basal sites of MoS_2 by impregnation method, which favored the adsorption of hydrogen on the S atoms and thus enhanced HER performance in both acidic and alkaline media [38]. By DFT calculations, Xu et al. predicted that the doped single Ni atoms influenced the extent of H coverage on the 1T-MoS_2 by weakening the strength of S-H bond, favoring H desorption and boosting HER activity [66].

By a solvothermal method, Xu et al. immobilized isolated Cu atoms into porous 1T-MoS_2, showing a low HER overpotential (η_{10}) of 131 mV at 10 mA·cm^{-2} in 0.5 M H_2SO_4 [67]. The isolated Cu ions are coordinated with S atoms, leading to numerous sulfur vacancies. Furthermore, electrons are preferably transferred from Cu to 1T-MoS_2, forming electron-rich MoS_2, which favored the desorption of H atoms and facilitated HER process. By high-throughput DFT simulations, Ma et al. predicted that isolated In/Ge doped S-defective MoS_2 could efficiently catalyze HER [68]. The electron donating effect of In/Ge atoms would raise the unoccupied anti-bonding orbital, modulate the desorption of H* intermediate and improve increase the conductivity of MoS_2, thus boosting HER activity.

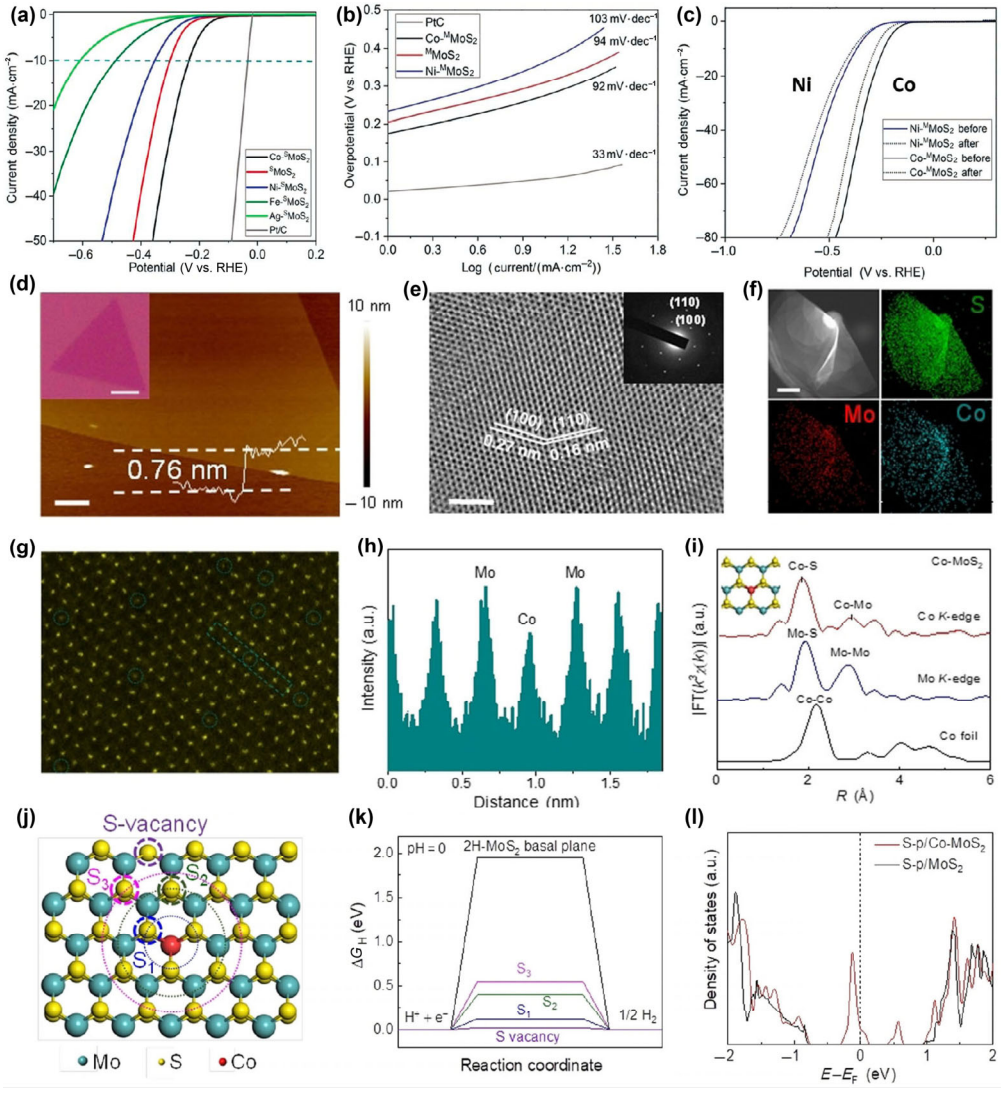

Figure 6 (a) LSV curves in 0.5 M H_2SO_4. (b) Tafel plots. (c) LSV curves of Co–^{S}MoS_2 and Ni–^{S}MoS_2 before and after 1,000 repeat scans [41]. (d) AFM image of Co-MoS_2 monolayer (Scale: 2 mm). (e) HRTEM image (Scale: 2 nm) and the corresponding SAED (inset). (f) EDX elemental mapping images (Scale: 500 nm). (g) HAADF-STEM image and (h) the intensity spectra of the selected area of Co-MoS_2 monolayer. (i) The FT curves of the Co K-edge and Mo K-edge EXAFS. (j) Structural model. (k) Free energy diagram for S atoms in the basal plane, S_1, S_2, S_3 and S vacancy. (l) Projected DOS of S atoms [42]. (a)–(c) Reproduced with permission from Ref. [41], © The Royal Society of Chemistry 2018. (d)–(l) Reproduced with permission from Ref. [42], © WILEY-VCH Verlag GmbH & Co. KGaA, Weinheim 2018.

Besides atomic non-noble metal doped MoS_2, precious metal doped MoS_2 also exhibited enhanced HER activity. By a sonication method, Tsang et al. anchored single-atom Pt or Pd onto 1T-MoS_2, displaying improved HER activity [69]. The recombination of H to H_2 can be accelerated on the isolated Pd site, thus promoting HER activity. By a hydrothermal method, Song et al. immobilized single-atom Pt onto ultrathin MoS_2, exhibiting an overpotential (η_{10}) of 180 mV for HER in 0.5 M H_2SO_4 [70]. The isolated Pt atoms absorbed on the surface of 1T-MoS_2 can capture H^+ ions, increasing active sites and boosting HER. The introduction of single-atom Ru onto MoS_2 would generate S vacancies, which lowered the reaction energy barrier and favored the adsorption/desorption of H* intermediate, thus enhancing HER activity [39]. Deng et al. anchored atomic rhodium onto MoS_2 using a solvothermal reaction, which a low overpotential (η_{10}) of 67 mV for HER in 0.5 M H_2SO_4 [40]. They found that a distance synergy between single-site Rh and adjacent in-plane S atoms could adjust the HER performance. Tan et al. anchored single-site Ru onto monolayer MoS_2 by an impregnation method, which exhibited a low HER overpotential (η_{10}) of 30 mV in 1 M KOH [71]. The introduction of single-site Ru resulted in bending strain of MoS_2, which enhanced reactant density in strained S vacancies and sped up HER on the Ru sites.

Due to high formation energy of 1T-WS_2, it is difficult to prepare highly pure 1T-WS_2 monolayers. Li et al. adopted a CVD method to synthesize single-atom V doped 1T-WS_2 monolayers with 91% phase purity for enhanced HER activity [72]. Through experimental and simulated STEM images, it can be observed that partial W sites were replaced by isolated V atoms with an average concentration of 4.0 at.%. Compared with pure 1T-WS_2, single-atom V doped 1T-WS_2 demonstrated lower HER overpotential (η_{10} = 185 mV) in acidic media. DFT calculations revealed that weaker H adsorption happened on the isolated V-S sites, leading to superior HER performance.

Through systematic DFT calculations, Liu et al. predicted that isolated Cr or V doped FeS_2 exhibited outstanding HER activity [73]. Single-atom Cr doped FeS_2 showed a low $|\Delta G_{H^*}|$ value of 0.049 eV and a low kinetic barrier of 0.22 eV for HER, which even surpassed the state-of-the-art Pt catalysts. Since H preferred to adsorb on the Cr atoms, they were regarded as the active sites.

Vanadium diselenide (VSe_2) is a member of the transition-metal dichalcogenides with a sandwich T-phase structure. Due to excellent conductivity, monolayer VSe_2 is a promising electrocatalyst for HER. Wang and co-workers found Fe-doped VSe_2 exhibited enhanced HER activity [74]. By simulating HER activity on a series of transition-metal atoms (Sc, Ti, V, Cr, Mn, Fe, Co, Ni, Cu, Zn, Ru, Rh, Pd, Os, Ir and Pt) doped VSe_2, Wang et al. predicted that single-atom Pt/Zn/Rh doped VSe_2 exhibited low theoretical overpotentials, which were expected as excellent HER electrocatalysts [75]. Gao et al. found that 1D-patterned VSe_2 can be reversibly transformed into monolayer VSe_2 by changing synthetic conditions [76]. After introducing Pt atoms, they were atomically adsorbed on the 1D-patterned VSe_2, which was calculated to be highly active for HER.

4.1.2 *Single metal atoms doped transition metal phosphides for HER*

In recent years, transition-metal phosphides (TMPs) have caught a great deal of attention for HER. However, compared with Pt-based catalysts, TMPs usually showed worse HER activity due to slower kinetics. To improve the HER activity, an efficient strategy is doping high-performance active metal atoms into the framework of TMPs. For instance, Chen and co-workers obtained atomically dispersed Ru on FeP by phosphating a Ru-doped FeOOH precursor as shown in Figs. 7(a)–7(d) [77]. One Ru cation was coordinated with four P atoms (Ru^{+3}-P_4-Fe configuration) and the average bond length for Ru-P was 0.237 nm, slightly longer than that (0.226) for Fe-P (Figs. 7(e)–7(h)). Compared with primary FeP nanorods, single-atom Ru decorated FeP showed a smaller overpotential (η_{10}) of 62 mV for acidic HER. A cooperation mechanism between Ru and Fe can enhance the hydrogen adsorption/desorption on the FeP substrate (Figs. 7(i)–7(m)), thus lowering HER energy barrier (only 0.5 eV) and boosting reaction kinetics. Song and co-workers incorporated single-atom Ru into Ni_5P_4 by phosphating a Ru-doped FeOOH precursor [78]. Compared with primary Ni_5P_4, single-atom Ru decorated Ni_5P_4 exhibited a lower overpotential (η_{10}) of 54 mV for alkaline HER (Figs. 7(n)–7(s)). The electron density of single-atomic Ru sites was improved by localized structural polarization, favoring H_2O dissociation and facilitating HER kinetics.

Luo and co-workers anchored isolated single-atom Pt onto CoP supported by a Ni foam via a potential-cycling method, which showed high HER activity and durability in neutral phosphate buffer solutions [79]. Liu et al. immobilized isolated single-atom Pt into the lattice of CoP nanosheets on carbon fiber cloth by chemical reaction of H_2PtCl_6 with CoP nanosheets at 30 °C, which exhibited outstanding electrocatalytic activity and durability for seawater electrolysis [80]. The d-band center of single-atom Pt in the lattice of CoP was calculated to be –4.39 eV, much smaller than that (–2.74 eV) of Pt (111), suggesting strong electronic interaction between isolated Pt and CoP. The free energy of H* ($|\Delta G_{H^*}|$) adsorbed on single-atom Pt modified CoP was 0.168 eV, larger than that (0.105 eV) on Pt (111). Wu et al. obtained single-atom W doped CoP nanoarrays by phosphating W-doped Co-MOF arrays, which exhibited excellent HER activity and good durability in acidic, basic, and neutral media [81]. The ΔG_{H^*} on the P site of W-CoP (111) surface was determined to be 0.069 eV, close to that of Pt(111) and smaller than that of the Mo-CoP (0.119 eV) and CoP (0.216 eV), indicating that the introduction of isolated W sites into CoP could decrease the HER energy barrier and facilitate HER kinetics.

4.1.3 *Single metal atoms doped (oxy)hydroxides for HER*

Although Pt shows excellent H_2 adsorption-desorption capacity, it displays poor activity for the dissociation of the H-O bond,

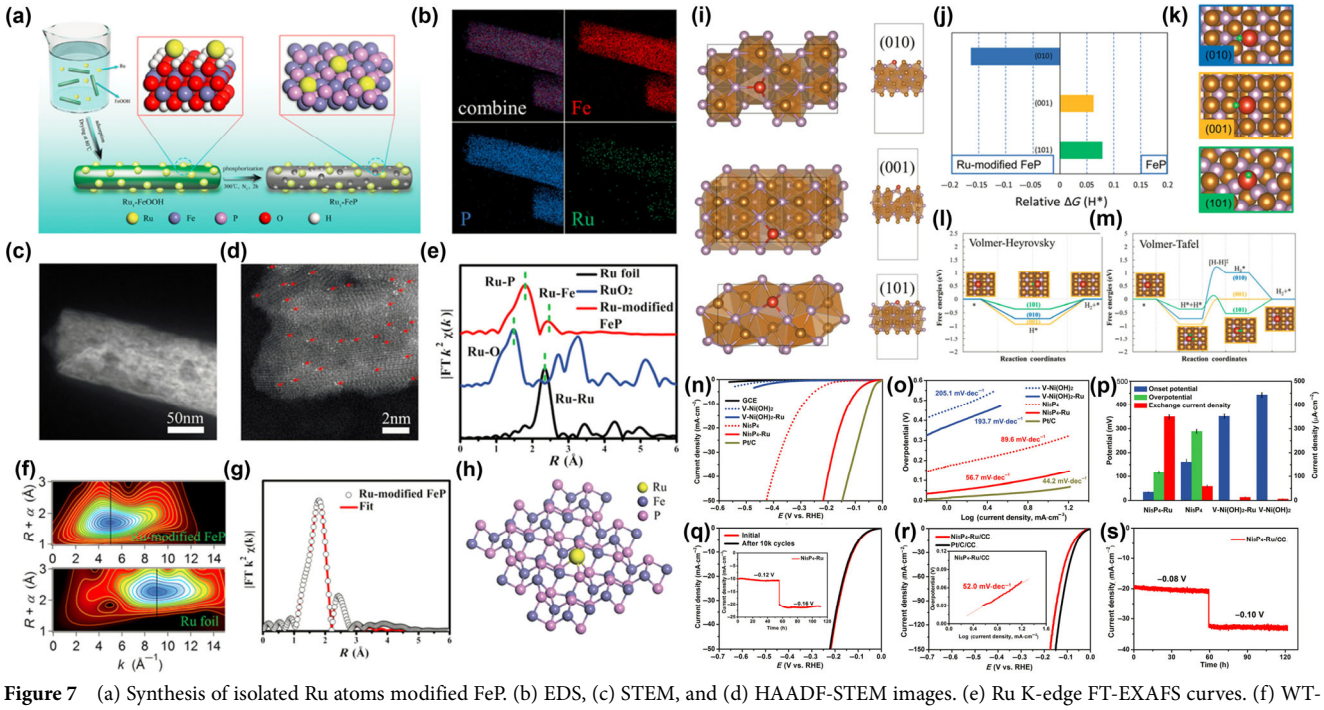

Figure 7 (a) Synthesis of isolated Ru atoms modified FeP. (b) EDS, (c) STEM, and (d) HAADF-STEM images. (e) Ru K-edge FT-EXAFS curves. (f) WT-EXAFS. (g) FTEXAFS fitting curves. (h) Atomic structure model. (i) Top and side views of Fe-exposed surfaces of FeP for the (010), (001) and (101) surfaces. (j) Relative ΔG_{H^*}. (k) Optimized structures of hydrogen adsorption. Energy diagrams of (l) Volmer–Heyrovsky and (m) Volmer–Tafel steps [77]. Color legend: Brown, Fe; light purple, P; red, Ru; green, H. (n) LSV curves. (o) Tafel slopes. (p) The calculated electrochemical parameters. (q) LSVs after long-term CV cycling and chronoamperometry measurement at given potentials measured for over 5 days. (r) LSV curves of samples loaded on carbon cloth collector, and the calculated Tafel slope. (s) Long-term stability measurement of Ni_5P_4-Ru loaded on carbon cloth [78]. (a)-(m) Reproduced with permission from Ref. [77], © Royal Society of Chemistry 2020. (n)-(s) Reproduced with permission from Ref. [78], © WILEY-VCH Verlag GmbH & Co. KGaA, Weinheim 2020.

which causes a large kinetic energy barrier for overall HER [82]. In the meantime, metal oxides or hydroxides showed excellent OER activity with low energy barrier for the dissociation of water [83]. Therefore, rational design of electrocatalysts combining the merits of Pt and oxides/hydroxides is expected to synergistically catalyze H-O bond cleavage, facilitate H-H bond formation, and thus improve the overall HER performance. Ni and co-workers anchored single-atom Pt onto partially amorphous NiRu-hydroxide by anodic oxidation of Pt electrode and cathodic reduction of produced Pt^{2+} [84]. The Pt/NiRu-OH exhibited high HER activity with a low overpotential (η_{10}) of 38 mV in 1 M KOH. Qiu et al. synthesized highly dispersed Pt (including single sites and clusters) in TiO_2 and CeO_2 nanowires by the dealumination of Al-Ti-Pt and Al-Ce-Pt precursors, which exhibited comparable HER activity with Pt/C catalysts [85]. However, they did not perform theoretical simulations to uncover the possible synergistic effect between single-site Pt and (oxy)hydroxide substrates. Deep understanding the synergistic mechanism between single-atom Pt and cobalt hydroxide support was proposed by Wang et al. [86]. They immobilized single-atom Pt onto cobalt hydroxide nanosheets supported by Ag nanowires (Pt_{SA}–$Co(OH)_2$@Ag NW), which showed a low overpotential (η_{10}) of 29 mV for HER in 1 M KOH (Figs. 8(a)–8(f)). By theoretical simulations, they proposed that the enhanced HER activity was attributed to the local tip-enhancement electric field at the platinum sites allured by the cobalt hydroxide and more d electron favoring H* and H_2O adsorption (Figs. 8(g)–8(k)).

By a photoactivation strategy, Wang and co-workers anchored single-atom Pt onto $RuCeO_x$ with outstanding HER activity

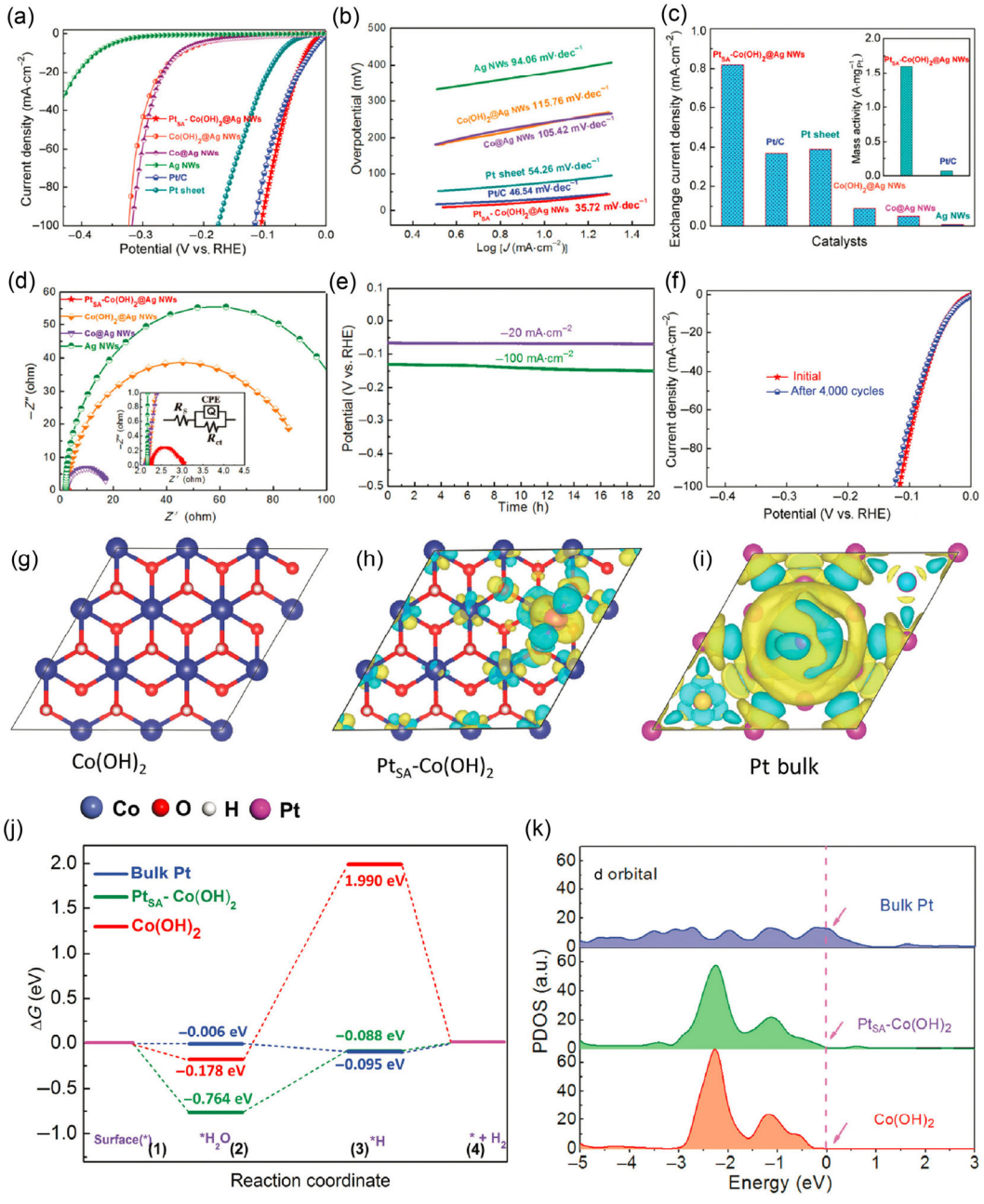

Figure 8 (a) LSV curves, (b) Tafel slopes and (c) exchange current densities of Pt_{SA}–$Co(OH)_2$@Ag NW, $Co(OH)_2$@Ag NW, Co@Ag NW, Ag NWs, the Pt sheet and Pt/C. (d) EIS Nyquist plots. Stability test of Pt_{SA}–$Co(OH)_2$@Ag NW via (e) chronoamperometry and (f) cyclic voltammetry measurements. (g) Top view of the slab models of $Co(OH)_2$. Top view of the calculated electron density difference of the Pt atom in (h) Pt_{SA}–$Co(OH)_2$, and (i) bulk Pt. (j) Calculated adsorption energies of H and H_2O. (k) Calculated PDOS of d orbitals [86]. (a)–(k) Reproduced with permission from Ref. [86], © The Royal Society of Chemistry 2020.

comparable to commercial Pt/C [87]. The Pt atoms were located in the lattice of RuO_2 and Pt-O-Ru bond was formed. Theoretical calculations revealed that multiple active sites might be responsible for superior HER activity, such as Pt sites in Cl-Pt-O-Ru and Pt-O-Ce, and O sites in Pt-O-Ru and Ce-O-Pt. Qiu and co-workers fabricated single atoms and Pt clusters doped TiO_2 or CeO_2 nanowires by a dealloying strategy [85]. Pt-TiO_2 or Pt-CeO_2 catalysts can be obtained by dealumination of Al-Ti-Pt and Al-Ce-Pt precursors in 2 M NaOH solution. After activation, the $Pt_{0.2}$-CeO_2 exhibited high acidic HER activity, which can be comparable with commercial Pt/C.

In the last few years, single-atom M-N-C catalysts have attracted much attention due to high electrocatalytic performance in many electrochemical reactions, especially in HER and ORR [19]. However, the carbon-based materials are instable under harsh conditions (e.g., high overpotentials, oxidative environment), which causes the leaching of active metal species from the substrate and catalyst deactivation. Oxides can be used in oxidative environment, which can support M-N moieties for electrocatalytic applications. Sun et al. supported PtN_x clusters with Pt–N coordination structure onto TiO_2 by N_2 plasma treatment of a Pt/TiO_2 precursor [88]. The PtN_x/TiO_2 showed a low HER overpotential (η_{10}) of 67 mV in 0.5 M H_2SO_4. DFT calculations revealed that the hydrogen adsorbed on N atoms would lead to a smaller ΔG_{H^*} than that adsorbed on Pt atoms.

4.1.4 *Single-site alloys for HER*

To decrease the usage of precious metals and improve their mass activity, two methods are commonly adopted: (i) aggrandizing available active sites and (ii) improving intrinsic activity of the active sites. Liu and co-workers fabricated a monolayer Pt on Ag/Au-coated Ni foam for efficient HER with an overpotential (η_{10}) of 100 mV in 0.5 M H_2SO_4 (Table 1) [89]. The Ag/Au coating on Ni foam was essential for ensuring complete-monolayer Pt coverage; otherwise, only partial monolayers were generated. Soon afterwards, Yau et al. deposited monolayer Pt on an Au(111) substrate by reduction of $PtCl_6^{2-}$ with CO, which exhibited higher hydrogen oxidation and evolution activity than Pt(111) [90]. Li et al. fabricated Cu-Pt dual sites alloyed with palladium nanorings by a two-step reduction of Cu^{2+} and Pt^{2+} on ultrathin Pd nanorings in solutions [91]. Surface d states of Pd nanorings were modulated by isolated single-atom Cu/Pt doping and strain effects, thus boosting the mass activity of precious metals. DFT calculations revealed that Pt was the active site for H atoms binding during HER, while adjacent Cu atoms could balance the adsorption of H* on Pt. Du and co-workers synthesized a RuAu single-atom alloy by laser ablation method with outstanding HER activity (η_{10} = 24 mV) [92]. According to the theoretical simulations, water molecules were absorbed and activated on the Ru sites, while the protons were absorbed on the Au sites and then H_2 was evolved. By theoretical calculations, Yang et al. predicted that Cu, Cr, Co, Ni, Mo, Rh, Ru, and Tc atoms doped PtTe sheets with Te-vacancies exhibited high HER activity due to ~ 0 eV of ΔG_{H^*} on the transition metal sites and adjacent Pt sites [93].

4.2 OER performance

4.2.1 *Single metal atoms doped transition metal (oxy)hydroxides for OER*

Although the electrocatalytic OER activity of iridium oxide is second only to ruthenium oxide among transition metal oxides, it is the most stable oxide electrocatalyst in acidic media. However, the scarcity and high price of iridium hinder the large-scale applications. Improving intrinsic activity of iridium sites by downsizing the particle size of iridium oxide to the atomic scale is highly preferred. One of the main issues for the applications of single-site catalysts is the leaching of isolated metal atoms from the support to the solution by surface etching or fracture of atomic bonds, which would lead to activity loss [35]. Moreover, aggregation of isolated metal atoms might happen under harsh reaction conditions if the interaction between the metal ions and support is not strong. Therefore, it is pivotal to fabricate SSCs with stable ligands and strong interaction of metal and support for practical applications. Song and co-workers prepared hierarchical CoIr catalysts with Co-Ir species by a reduction method using sodium borohydride as the reduction agent [36]. The CoIr with 9.7 wt.% Ir content displayed excellent OER activity with an overpotential (η_{10}) of 373 mV 1 M phosphate buffer solution. Soon afterwards,

Table 1 Comparison of HER performance of carbon-free single-site catalysts

Catalyst	Electrolyte	η@10 mA·cm^{-2} (mV)	Tafel slope (mV·dec^{-1})	Ref.
Ag@MoS_2 core-shell	0.5 M H_2SO_4	195.7	41.1	[62]
Co-MoS_2	0.5 M H_2SO_4	137	64	[42]
Co-^{S}MoS_2	0.5 M H_2SO_4	220	92	[41]
SA Co-D 1T MoS_2	0.5 M H_2SO_4	100	32	[47]
Co_1/MoS_2	0.5 M H_2SO_4	212	76	[64]
Cu@MoS_2	0.5 M H_2SO_4	131	51	[67]
Pd/Cu-Pt NRs	0.5 M H_2SO_4	22.8	25	[91]
Fe-doped VSe_2	0.5 M H_2SO_4	390	112	[74]
MCM@MoS_2-Ni	0.5 M H_2SO_4	161	81	[65]
Ni_{SA}-MoS_2	0.5 M H_2SO_4	110	74	[38]
Ag@PdAg	0.5 M H_2SO_4	—	70	[94]
Pt/NiS@Al_2O_3	0.5 M H_2SO_4	34	35	[95]
Pt-1T′ MoS_2	0.5 M H_2SO_4	180	88.4	[70]
Pt/$RuCeO_x$-PA	0.5 M H_2SO_4	45	31	[87]
PtN_x/TiO_2	0.5 M H_2SO_4	67	34	[88]
Pt/AuNF/Ni foam	0.5 M H_2SO_4	100	53	[89]
Rh-MoS_2-4.8	0.5 M H_2SO_4	67	54	[90]
Ru-modified FeP	0.5 M H_2SO_4	62	45	[77]
V SACs@1T-WS_2	0.5 M H_2SO_4	185	61	[72]
W-CoP	0.5 M H_2SO_4	48	56	[81]
$Pt_{0.2}$-CeO_2	0.5 M H_2SO_4	—	35	[85]
Mo-Co_9S_8@C	0.5 M H_2SO_4	98	34.6	[96]
Ni_{SA}-MoS_2	1 M KOH	98	75	[38]
1T-^{S}MoS_2	1 M KOH	—	61	[69]
Pt/NiRu-OH	1 M KOH	38	39	[84]
Pt SA–Co$(OH)_2$@Ag	1 M KOH	29	35.72	[86]
Pt_{at}–CoP MNSs/CFC	1 M KOH	13	30.28	[80]
Ru/np-MoS_2	1 M KOH	30	31	[71]
5.0%-Ru-MoS_2	1 M KOH	76	21	[39]
RuAu-0.2	1 M KOH	24	37	[92]
Ni_5P_4-Ru	1 M KOH	54	52	[78]
STRO	1 M KOH	46	40	[97]
W-CoP	1 M KOH	36	47	[81]
Rh SAC–CuO NAs/CF	1 M KOH	44	—	[98]
Pt/np-$Co_{0.85}Se$	1 M PBS	19	35	[99]
W-CoP	1 M PBS	~ 21	81	[81]
PtSA-NT-NF	1 M PBS	24	30	[79]

Gu et al. anchored isolated Ir atoms onto amorphous CoO_x nanosheets by the same reduction method, which exhibited superior OER activity with a ultra-low overpotential (η_{10}) of 152 mV in 1 M KOH [37]. Although these single-site Ir-based catalysts showed outstanding OER performance, the authors did not perform theoretical studies to reveal the reaction mechanism. More in-depth work was carried out by Wang and co-workers [100]. They anchored single-site Ir onto cobalt nanosheets with dual-reactive Ir-Co sites for efficient OER in alkaline media. Combining DFT calculations with experimental results, they found that the OOH* intermediate can be better stabilized on the Co-O-Ir site due to a strong hydrogen bonding interaction.

In addition, the Pearson absolute electronegativity (χ) of iridium is 5.4 eV, which is larger than that of Co (4.3 eV) and Ni (4.4 eV) [101]. The electronic structures of Co and Ni can be modulated by introducing Ir atoms into the (oxy)hydroxide systems, leading to the formation of highly charged Co and Ni species with lower overpotentials for OER. Therefore, it is expected that the OER activity of Ni-based (oxy)hydroxides can also be improved by introducing isolated Ir sites. Chen et al. synthesized atomic Ir doped nickel hydroxide nanosheets using hexamethylenetetramine as the hydrolysis reagent to hydrolyze H_2IrCl_6 and $NiCl_2$ in an ethanol solution [102]. Compared with IrO_2 (η_{10}: 332 mV) and Ir-free $Ni(OH)_2$ (η_{10}: 359 mV), Ir-$Ni(OH)_2$ with 4 wt.% Ir showed lower overpotential (η_{10}: 235 mV) for alkaline OER. The inductive effect between Ni and Ir promoted the formation of highly charged Ni species, which favored the adsorption of nucleophilic intermediates, thus boosting the OER performance. In addition, the OER activity of porous $NiCo_2O_4$ nanosheets can be enhanced by introducing isolated Ir sites. For example, Xi et al. anchored atomic Ir onto ultrathin porous $NiCo_2O_4$ nanosheets by an electrodeposition method (Figs. 9(a)–9(h)), which showed a low OER overpotential (η_{10}: 240 mV) and 70 h of stability in 0.5 M H_2SO_4 [103]. DFT calculations revealed that the enhanced OER activity should be ascribed to the improved surface electronic electron exchange and transfer ability on the isolated Ir sites couplings with oxygen vacancies on the surface of $NiCo_2O_4$ (Figs. 9(i)–9(k)).

Besides single-site Ir doping, atomic Pt doping can also improve the OER activity of NiO. Lin and co-workers

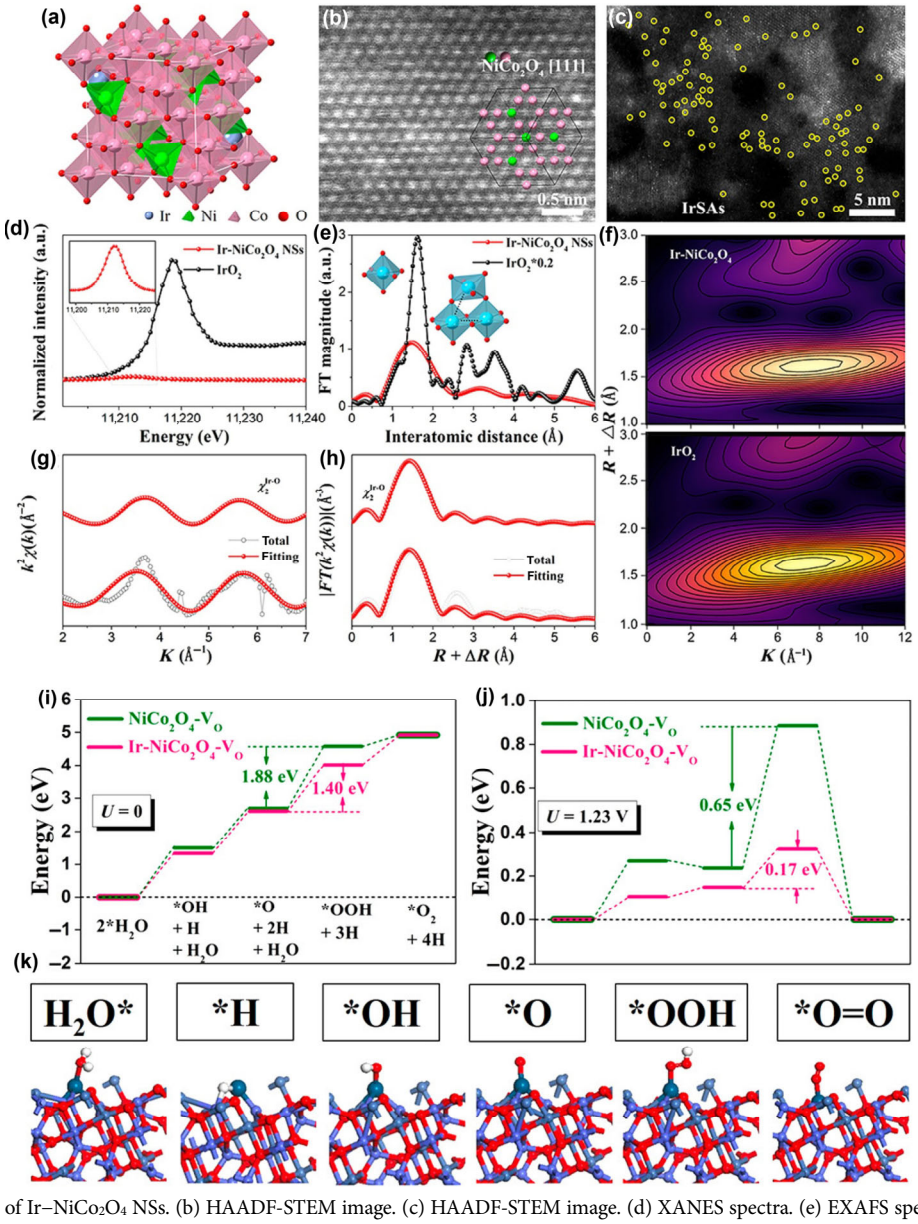

Figure 9 (a) Structure of Ir–$NiCo_2O_4$ NSs. (b) HAADF-STEM image. (c) HAADF-STEM image. (d) XANES spectra. (e) EXAFS spectra. (f) Corresponding wavelet transforms for the k^3-weighted Ir L_3-edge EXAFS signals. (g) and (h) Ir L_3-edge EXAFS. (i) The pathways at U = 0 V. (j) The OER pathways at U = 1.23 V. (k) Local structural configurations [103]. (a)–(k) Reproduced with permission from Ref. [103], © American Chemical Society 2020.

immobilized atomic Pt onto porous NiO nanocubes by an atomic layer deposition method, which exhibited enhance OER activity compared with pristine NiO [43]. Different from atomic Ir as the active site for OER, the isolated Pt cannot serve as the active sites directly. By theoretical studies, they proposed that the role of atomic Pt was to facilitate phase transformation by lowering the migration barrier of adjacent Ni sites. However, it should be considered that Pt atoms will be dissolved into the electrolytes under the OER conditions.

Due to poor electroconductivity of Fe-based oxides, they usually show high overpotentials for OER. However, Fe-doping into Co-based and Ni-based (oxy)hydroxides can significantly promote the OER due to a collaborative mechanism between Fe and Co/Ni sites [104]. Recently, Zhang and co-workers found that the OER performance of cobalt carbonate hydroxide hydrate can be distinctly improved by doping single Fe atoms [105]. DFT calculations revealed that the electron would transfer from Fe sites to the adjacent Co sites, leading to electron-rich Co sites and lower energy barrier (1.52 eV) than that (1.71 eV) on Fe-free Co sites for OER. The formation of OOH* intermediate was predicted to be the potential-determining step. Previous studies found that the Fe sites in (Ni,Fe)OOH should be the active sites for OER [106], but then a growing body of evidence pointed to the Ni sites as the active sites [107, 108]. Recent theoretical calculations also supported that the OER active sites should be Ni sites, while the role of Fe might be increasing and stabilizing the reactive phases [104].

Trimetallic FeCoNi (oxy)hydroxides are superior electrocatalysts for the OER in alkaline media. Further improving their OER activity is very challenging. Very recently, Wu and co-workers synthesized a Ru-doped FeCoNi-based metal organic framework by an ion exchange method, which can be transformed into an layered double hydroxide (LDH) [109]. Isolated Ru sites on the amorphous outer layer favored the formation of Ru-O* intermediate, boosting the OER kinetics. The Ru SAs/AC-FeCoNi hybrid material exhibited a low overpotential (η_{10}) of 205 mV in 1 M KOH (Table 2). In addition, the OER activity of cobalt-iron layered double hydroxides can be also improved by atomic Ru-doping. Li et al. anchored single-site Ru (0.45 wt.%) onto CoFe-LDHs by a precipitation method, which exhibited a ultra-low overpotential (η_{10}) of 198 mV in 1 M KOH [110]. By operando XAS, they found that the valence state of Ru was kept 4+ during the OER process due to strong synergetic electron coupling between single-site Ru and CoFe-LDHs. The avoiding generation of highly charged Ru ions would prevent them from dissolving in the electrolyte and thus improve the stability. Moreover, Huang et al. found that atomically dispersed Ru can be embedded into the lattice of CoCr LDHs by simple coprecipitation process [111]. The CoCrRu LDHs showed a low overpotential (η_{10}) of 290 mV for the OER in 0.1 M KOH. The atomic Ru doping can reduce d-band center value of Co and improve electron donation of Cr to oxygenates, thus lowering the OER energy barrier.

Nickel oxide has been regarded as the most active non-noble metal oxide catalyst for OER in basic media [108]. Tremendous efforts have been dedicated to enhanced its OER activity, including downsizing the nanoparticles, increasing specific surface area, and Fe-doping strategy. Baeumer and co-workers studied the OER performance on atomically flat $LaNiO_3$ thin films and found that the Ni termination was active, while the La termination was kinetically inaccessible, indicating that Ni atom is the active site for OER [112]. To improve OER performance of Ru-based catalysts, Kim and co-workers synthesized a core–shell single-atom Ni catalyst Ni-Ru@RuO_x-HL with metal Ru as the core and NiO and RuO_x as the shell by an acid-leaching method, which exhibited low overpotentials of 184 and 229 mV at 10 and 100 mA·cm^{-2} in 0.5 M H_2SO_4 (Fig. 10) [113]. There was negligible dissolution of Ni and Ru for the Ni-Ru@RuO_x-HL catalyst during OER stability test, indicating stable active sites. The theoretical overpotentials on RuO_2 containing two metal ion vacancies at coordinatively unsaturated sites and two Ni-atom doping at bridge sites were calculated to be 0.211 and 0.191 V for adsorbates evolution mechanism and acid-base lattice oxygen mechanisms, respectively. The shorter Ru-O bonds favored acid-base O–O bond formation.

Cobalt oxide is an excellent electrocatalyst for alkaline OER. Compared with bulk Co_3O_4, ultrafine CoO_x nanoparticles exhibited higher OER activity [114]. Further downsizing the CoO_x nanoparticles to single Co sites still exhibited OER activity. Very recently, Zhang and co-workers immobilized single-atom Co into TiO_2 nanorods by an organic colloidal solution [115]. The Co-TiO_2 with 12% Co showed an overpotential (η_{10}) of 332 mV for OER in 1 M KOH and a turnover frequency of 6.6 ± 1.2 s^{-1} at an overpotential of 300 mV. Compared with Fe-TiO_2 and Ni-TiO_2, the isolated Co sites in Co-TiO_2 performed the O–O coupling step with a smaller energy barrier, thus showing higher OER activity.

4.2.2 *Single metal atoms doped transition metal dichalcogenides/phosphides for OER*

Although TMPs have been widely investigated for HER, they were seldom applied in OER since they would gradually transform to corresponding oxides under extremely oxidizing conditions. For instance, Tan and coworkers found that the surface of nanoporous $(Ni_{0.74}Fe_{0.26})_3P$ would reconstruct to form an amorphous Ni(Fe) oxyhydroxide under electrochemical OER conditions [116]. After the deprotonation process during OER, partial isolated Ir sites were reunited to form multiple active sites, facilitating the O–O coupling. Improving the OER activity to lower applied overpotentials can prolong the working life of TMPs for OER. Gu et al. found that Au atoms would diffuse from Au yolks into the Ni_2P shell under high temperature (≥ 350 °C) treatment [117]. After doping single Au atoms/clusters, the volume of Ni_2P shell would expand and the OER activity can be significantly enhanced with a low overpotential (η_{10}) of 240 mV in 1 M KOH. Moreover, as mentioned above, the MoS_2 monolayer can be served as a two-dimensional substrate to support isolated metal atoms for enhanced HER performance [63]. However, there are seldom experimental reports about single metal atoms doped transition metal dichalcogenides for the OER mainly due to their poor stability under harsh oxidizing conditions. By theoretical investigations, Zhao et al. predicted that Pd_2 nanoclusters incorporated on the defective MoS_2 monolayer with S vacancies exhibited a low overpotential of 0.32 V for OER [118].

4.2.3 *Single-site alloys for OER*

The main issue for catalyst degradation in the OER is the dissolution of active metal components in acidic media. Although RuO_2 is the most active monometallic oxide catalyst for the OER in acidic conditions, the over-oxidation of Ru to $Ru^{>4+}$ species by adsorbate evolution mechanism or lattice OER would lead to the dissolution of Ru into the electrolyte and catalyst deactivation [119–121]. Therefore, it is necessary to modulate the geometric and electronic structure of Ru to prevent its dissolution [122]. Compared with Ru, metallic Pt possesses a slower dissolution rate in acidic media due to the worse oxygen bonding ability. Immobilization of isolated Ru atoms into the crystal lattice of Pt would favor the improvement

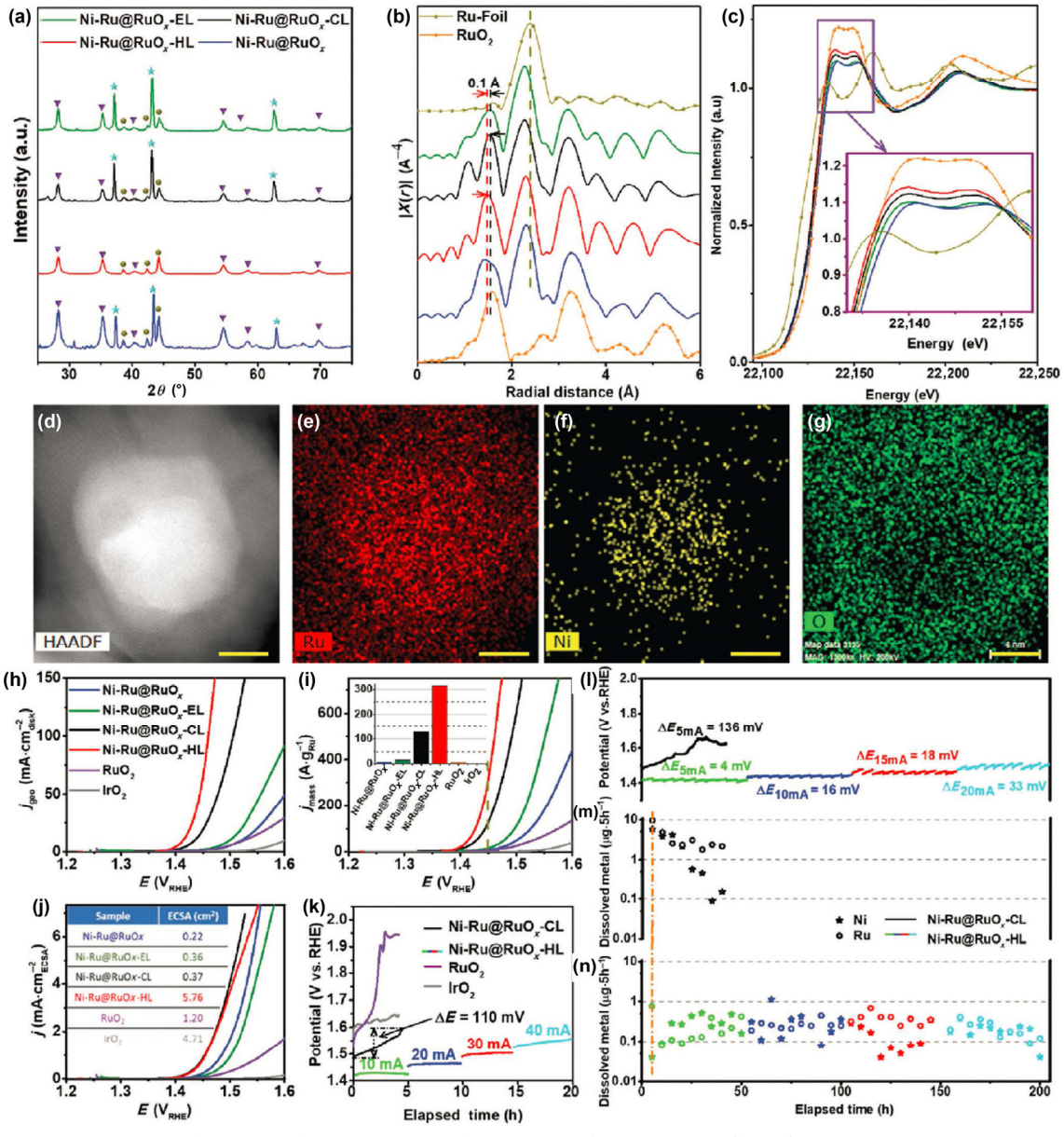

Figure 10 (a) XRD patterns, (b) Ru K-edge FT-EXAFS, and (c) Ru K-edge XANES profiles of Ni-Ru@RuO$_x$-EL, Ni-Ru@RuO$_x$-CL, and Ni-Ru@RuO$_x$-HL. (d)–(g) HAADF-STEM image and STEM-EDS elemental mapping of Ni-Ru@RuO$_x$-HL (scale bars: 6 nm). (h) LSV curves in 0.5 M H_2SO_4. (i) Mass activity profiles. Inset shows the histogram of mass activity at 1.45 VRHE. (j) ECSA corrected activity profiles. (k) Chronopotentiometric plots at 10 (green), 20 (blue), 30 (red), and 40 (sky blue) mA·cm^{-2} for Ni-Ru@RuO$_x$-HL. (l) Stability outlines and (m,n) dissolution profiles [113]. (a)-(n) Reproduced with permission from Ref. [113], © Wiley-VCH Verlag GmbH & Co. KGaA, Weinheim 2021.

of dissolution resistance of Ru. Wu and co-workers embedded atomically dispersed Ru into PtCu alloys by acid etching and subsequent electrochemical leaching strategy, which showed higher OER activity and durability than commercial RuO_2 [123]. Theoretical studies revealed that the electronic structure of isolated Ru was engineered by the compressive strain of the Pt substrate, which favored binding oxygen species and improved the resistance to over-oxidation and dissolution.

4.2.4 Single metal atoms doped borophene or boron phosphides for OER

As a member of the family of two-dimensional materials, borophene has attracted many interests due to the abundant polymorphism properties. However, the large-scale synthesis of borophene is still challenging by far due to harsh synthetic conditions. For instance, in an ultrahigh vacuum condition, borophene with different structures can be generated on the surface of Ag (111), Cu (111), Au (111), and Al (111) [124–127]. Therefore, the research work about borophene for electrocatalysis is mainly focused on theoretical simulations. For example, Ahuja et al. predicted that Ti-functionalized borophene monolayer showed higher HER and OER activity on than the pristine borophene since the introduction of isolated Ti atoms would increase the average buckling height and change the charge density distribution of the borophene [128]. Mohajeri and Dashti predicted that Ni-doped B_{36} and Ti-doped B_{36} showed higher OER and HER activity than pristine B_{36}, respectively [129]. Additionally, they proposed that the intermetallic cooperativity effect in dual-metal FeNi-codoped B_{36} favored bifunctional OER and HER. The isolated Fe site was responsible for OER, while the Ni site was in charge of OER. By DFT simulations, Jung et al. found that the density of states near the Fermi-level of isolated Rh and Co sites in Rh–BH and Co–BH can be increased due to the coupling of d-orbitals of the Rh and Co dopants with the p-orbitals of adjacent boron atoms (Fig. 11) [130]. The predicted theoretical

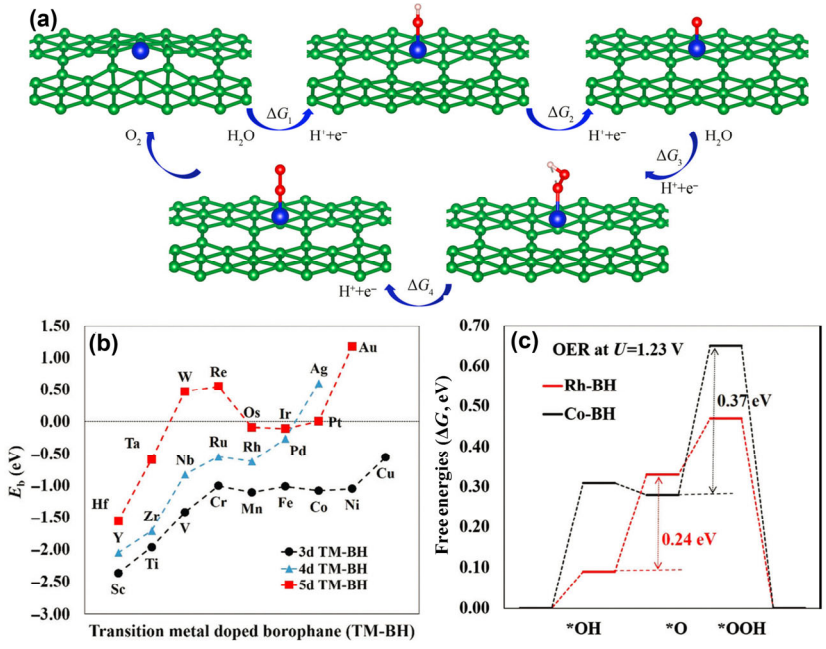

Figure 11 (a) Proposed 4e⁻ reaction scheme for OER. (b) Binding energies of various transition metals embedded into the borophene matrix. (c) The reaction free energy diagram of the OER on Co–BH and Rh–BH. (a) Reproduced with permission from Ref. [131], © Xu, X. et al. under exclusive licence to Springer-Verlag GmbH, DE part of Springer Nature 2021. (b) and (c) Reproduced with permission from Ref. [130], © The Royal Society of Chemistry 2018.

OER overpotentials on Rh–BH and Co–BH were 0.24 and 0.37 V, respectively, which were lower than that on rutile-type RuO_2 (0.37 V). In addition, Xu et al. predicted that the theoretical OER overpotentials on the β_{12}–Ni and χ_3–Ni (β_{12} and χ_3: two types of borophene) were 0.38 and 0.35 V, respectively [131]. However, although theoretical studies predicted that single metal atoms incorporated into borophene are structurally and thermodynamically stable, the practical stability of M-B bonds under harsh OER conditions should be experimentally verified. In addition to borophene, N-doped boron phosphides (BP) can be also utilized as two-dimensional substrates to support isolated metal sites for efficient OER. Lau and co-workers predicted that the theoretical OER overpotentials on CoN_3-BP, NiN_3-BP, and PtN_3-BP were 0.42, 0.44, and 0.25 V, respectively. However, the stability of M-P bonds in these catalysts should be challenging under harsh oxidizing conditions [132].

4.3 Bifunctional HER/OER performance

Due to different reaction mechanisms, an active site usually cannot simultaneously catalyze bifunctional HER and OER. For example, although Pt catalysts are highly active for HER, they show very poor OER activity. Iridium oxide can efficiently catalyze OER, but it exhibits poor HER activity [133]. It is challenging for an active site with appropriate adsorption-desorption capacity of both H* and OH* species, which is the key intermediate for HER and OER, respectively. There are three main methods for fabricating bifunctional HER and OER catalysts. The first one is rationally regulating the coordination environment of isolated metal sites to moderately adsorb and desorb the H* and OH* intermediates. The second one is supporting isolated metal sites on a suitable substrate with synergistic mechanism to catalyze HER and OER. The last one is fabricating dual-metal sites for synergistically catalyzing HER and OER.

By first-principles simulations, Wang et al. predicted that single-site Ni embedded on β_{12} boron monolayer (Ni_1/β_{12}-BM) possessed excellent HER and OER activity with a low theoretical overpotential of 0.06 and 0.4 V, respectively [134]. The improved HER performance of Ni_1/β_{12}-BM was assigned to a cooperation mechanism of the tensile strain by incorporating Ni atoms onto the boron monolayer and charge transfer between isolated Ni sites and boron monolayer. However, for all I know so far, there are no related experimental reports about carbon-free single-site Ni catalysts with bifunctional HER and OER activity.

As mentioned above, transition metal dichalcogenides exhibited excellent HER activity, but poor stability for OER. Sun and co-workers found that doping single-site Mo onto Co_9S_8 nanoflakes can not only improve the HER and OER activity, but also prolong the durability [96]. They anchored atomic Mo onto partially oxidized surface sulfur sites by a two-step solvothermal process, which exhibited outstanding overall water splitting activity with overpotentials of 1.68 and 1.56 V in acidic and alkaline media, respectively. No obvious decay in activity can be observed for continuous operation of 24 h in 0.5 M H_2SO_4 and 72 h in 1 M KOH (Fig. 12). Theoretical studies revealed that the adsorption energy of H_2O molecules on the Co sites was modulated an ideal value by introducing atomic Mo and the theoretical OER overpotential on the Mo-Co_9S_8@C was lowered to be 0.41 V, indicating that a cooperation mechanism between isolated Mo and Co sites existed during the OER process. In addition, by DFT simulations, Cheng et al. predicted that single-site Pt anchored on MoS_2 edge sites exhibited low theoretical overpotentials for HER (0.1 V) and OER (0.46 V) [135]. Han et al. predicted that single-site Pt doped $NbSe_2$ and TaS_2 were suitable electrocatalysts for bifunctional HER and OER [136]. They also calculated the durability of single atom doped transition metal dichalcogenides by the difference ($\Delta E = E_b - E_{coh}$) in binding energy (E_b) and cohesive energy (E_{coh}), and found the ΔE of these catalysts was smaller than 0.15 eV, suggesting their structural stability for overall water splitting.

For practical application in electrocatalytic water splitting, the catalysts should possess structural stability and outstanding durability. Comparatively speaking, metal (oxy)hydroxides are more stable than metal dichalcogenides/phosphides under

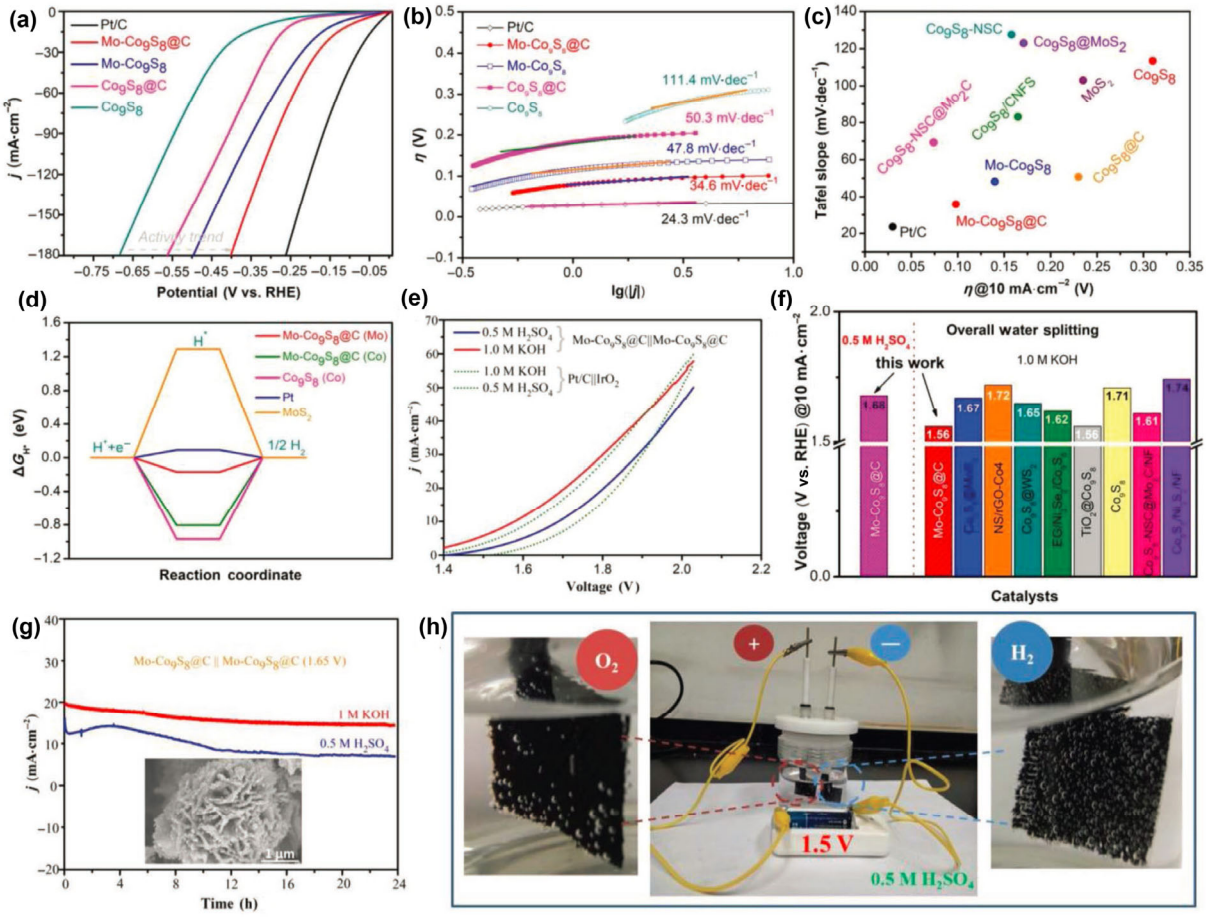

Figure 12 (a) HER polarization curves. (b) Tafel plots. (c) Comparison of overpotential. (d) The free-energy diagram for HER. (e) Overall water splitting performance. (f) Full water splitting potentials. (g) Durability test for the Mo-Co_9S_8@C. (h) Optical photograph of overall water splitting using Mo-Co_9S_8@C/CC. (a)–(h) Reproduced with permission from Ref. [96], © WILEY-VCH Verlag GmbH & Co. KGaA, Weinheim 2019.

OER condition. Precious metal Ru showed excellent HER activity, while NiFe layered double hydroxide (LDH) exhibited outstanding OER activity. It is expected that single-site Ru immobilized into NiFe LDH would bifunctionally catalyze HER and OER. Wang et al. found that the Ru–NiFe LDH on Ni foam showed superior HER and OER activity with a low overpotential (η_{10}) of 116 and 230 mV, respectively (Table 2) [137]. DFT calculations uncovered that the introduction of Ru into NiFe LDH can lower the adsorption energy of H* and increase the adsorption energy of OH* on the catalyst surface, thus promoting HER and OER. Huang et al. immobilized atomic Rh onto CuO nanowire arrays on copper foam by a cation exchange method [98]. Compared with Rh nanoparticles, the Rh SAC-CuO NAs/CF catalyst showed higher HER and OER activity. It can be used as bifunctional electrocatalysts for overall water splitting with a low overpotential of 1.51 V to reach 10 mA·cm^{-2} in 1 M KOH. DFT calculations revealed that the enhanced HER and OER activity resulted from moderate adsorption energy of reaction intermediates on the atomic Rh sites.

5 Summary and outlook

In this review, we have systematically summarized the recent progress in fabricating carbon-free single-site catalysts for HER, OER and overall water splitting. Although dozens of synthetic methods have been developed for the fabrication of single-site catalysts till now, only a few preparation methods (e.g., wet chemistry method, hydrothermal synthesis, and chemical vapor deposition) were adopted for the construct of carbon-free single-site catalysts for HER and OER. The loading density of single metal sites in the single-site catalysts is relatively low, which limits their practical application. In addition, compared with carbon-based materials, carbon-free supports usually show lower specific surface area, resulting in more difficulty to immobilize high-density isolated single atoms. Therefore, the development of a universal method to anchor high density of metal atoms onto carbon-free porous supports or two-dimensional materials with atomically dispersed and methodically regulable active sites is highly desirable for clean energy applications.

Compared with pristine supports, the enhanced electrocatalytic activity of carbon-free single-site catalysts comes from the following three aspects. (I) The doped single metal sites themselves exhibit high HER or OER activity. For example, TiO_2 nanorods show poor OER performance, while the OER activity can be significantly improved by incorporating isolated Co sites into the lattices. (II) A synergistic reaction mechanism between the doped single metal sites and the support boosts electrocatalytic performance. For instance, the enhanced HER activity of single-site Pt decorated $Co(OH)_2$ was ascribed to the local tip-enhancement electric field regions around the Pt sites induced by the $Co(OH)_2$ substrate. (III) The doped isolated metal sites lead to the lattice strain of supports, thus promoting electrocatalytic performance. Many experiments have verified that isolated single transition metal atoms embedded into the lattice of MoS_2 would lead to the lattice strain, which would enhance the reactant density in strained S vacancies, thus facilitating HER. These findings provide guidance for rational design of high-performance

Table 2 Comparison of OER performance of carbon-free single-site catalysts

Catalyst	Electrolyte	η@10 mA·cm^{-2} (mV)	Tafel slope (mV·dec^{-1})	Ref.
Au@Ni_2P-350 °C	1 M KOH	240	58	[117]
Co@MoS_2-500	1 M KOH	270	74	[138]
Co-TiO_2 (12% Co)	1 M KOH	332	72	[115]
Fe-CCHH/NF-30	1 M KOH	200	50	[105]
$Ir_1Co_{13.3}O_{20.1}$ANSs	1 M KOH	30	60.5	[37]
Ir@Co	1 M KOH	273	99	[100]
4% Ir-Ni(OH)$_2$	1 M KOH	235	58.4	[102]
$Ir_{18\ wt.\%}$-NiO	1 M KOH	215	38	[139]
np-Ir/NiFeO	1 M KOH	197	29.6	[116]
0.5 wt.% Pt/NiO	1 M KOH	358	33	[43]
Ru/CoFe-LDHs	1 M KOH	198	39	[110]
Ru SAs/AC-FeCoNi	1 M KOH	205	40	[109]
Ru/NiFe LDH-F/NF	1 M KOH	230	50.2	[137]
Rh SAC-CuO NAs/CF	1M KOH	197	71.7	[98]
Mo-Co_9S_8@C	1 M KOH	200	95.6	[96]
CoCrRu LDHs	0.1 M KOH	290	56.12	[111]
FeO_x/NF-Li	1 M NaOH	276	102	[140]
Mo-Co_9S_8@C	0.5 M H_2SO_4	370	90.3	[96]
Ir–$NiCo_2O_4$ NSs	0.5 M H_2SO_4	240	60	[103]
Ni-Ru@RuO_x-HL	0.5 M H_2SO_4	184	—	[113]
Ru_1–Pt_3Cu	0.1 M $HClO_4$	90	—	[123]
Ru-SA/$Ti_3C_2T_x$	0.1 M $HClO_4$	290	37.9	[141]
CoIr-0.2	1 M PBS	373	117.5	[36]

single-site catalysts for electrocatalytic applications.

Currently, the main bottleneck of carbon-free single-site catalysts for overall water splitting is the insufficient stability of isolated metal sites during long-running process under high current densities, especially for the anodic OER operated in oxidizing conditions. To improve the durability of single-site electrocatalysts for HER and OER, the following possible strategies can be considered. (I) The active metal sites can be properly selected from HER/OER volcano plots. (II) The active metals with high resistance to leaching should be reasonably chosen for HER/OER in different electrolytes. (III) Highly stable supports favor the long-running electrocatalytic operations. (IV) The isolated metal atoms should be incorporated into the lattice of carbon-free supports, not suspended on the surface. (V) The H* adsorption Gibbs free energies and desorption of H_2 molecules on the surface of single-site catalysts can be optimized for HER. (VI) The binding energies of the reaction intermediates (e.g., O*, OH*, and HOO*) on the surface of single-site catalysts for OER should be optimized. (VII) The desired single-site catalysts should possess good charge-transfer and mass-diffusion ability during HER/OER. (VIII) Single-site catalysts with large surface area and abundant active sites can facilitate HER/OER and prolong the durability. (IX) Rational design of single-site catalysts with stable active sites by theoretical simulations. Here we specially emphasize that the strong binding force between isolated metal atoms and the coordinating ligands attached to the substrate is vital for maintaining the stability of active sites away from aggregating and leaching during electrocatalytic HER/OER. For designing OER electrocatalysts, we should select supports with good electrochemical stability as far as possible, while for designing HER electrocatalysts, more attention could be devoted to seeking supports with high specific surface area and good electrical conductivity. So far, isolated metal atoms immobilized into the crystal lattice of two-dimensional MoS_2 might be suitable for HER, while single metal atoms doped ultrathin Fe-Co-based or Fe-Ni-based (oxy)hydroxide nanosheets should be promising for OER.

Finally, since the atomic number of many doped single metal atoms is close to that in the support, it is very hard to distinguish them directly from electron microscopes, which brings difficulties to *in-situ* monitor the dynamic process of active sites during electrocatalytic reactions. The XAS is a very powerful technique to characterize the geometric and electronic structure of the active sites, especially *in-situ* XAS can provide valuable dynamic information of active sites during HER/OER. However, due to ultrahigh cost of the large-scale XAS equipment, it is challenging to perform *in-situ*/operando studies for many researchers. Therefore, it is urgent to develop more easily available techniques for *in-situ* characterization of isolated single metal sites to better understand the reaction mechanisms. Despite many challenges ahead, ongoing efforts have been devoted to the single-site catalysis field over the past years, which will contribute to developing high-performance single-site catalysts for electrocatalytic applications and other catalytic reactions.

Acknowledgements

This work was supported by the National Natural Science Foundation of China (No. 22075099), and Natural Science Foundation of Jilin Province (No. 20180101291JC).

Conflict of interest

The authors declare no conflict of interest.

References

[1] Sultan, S.; Tiwari, J. N.; Singh, A. N.; Zhumagali, S.; Ha, M.; Myung, C. W.; Thangavel, P.; Kim, K. S. Single atoms and clusters based nanomaterials for hydrogen evolution, oxygen evolution reactions, and full water splitting. *Adv. Energy Mater.* **2019**, *9*, 1900624.

[2] Zhu, C. Z.; Fu, S. F.; Shi, Q. R.; Du, D.; Lin, Y. H. Single-atom electrocatalysts. *Angew. Chem., Int. Ed.* **2017**, *56*, 13944–13960.

[3] Han, X. B.; Wang, D. X.; Gracia-Espino, E.; Luo, Y. H.; Tan, Y. Z.; Lu, D. F.; Li, Y. G.; Wågberg, T.; Wang, E. B.; Zheng, L. S. Fe-substituted cobalt-phosphate polyoxometalates as enhanced oxygen evolution catalysts in acidic media. *Chin. J. Catal.* **2020**, *41*, 853–857.

[4] Li, Y. J.; Sun, Y. J.; Qin, Y. N.; Zhang, W. Y.; Wang, L.; Luo, M. C.; Yang, H.; Guo, S. J. Recent advances on water-splitting electrocatalysis mediated by noble-metal-based nanostructured materials. *Adv. Energy Mater.* **2020**, *10*, 1903120.

[5] Sun, W. J.; Meng, X. Y.; Xu, C. J.; Yang, J. Y.; Liang, X. M.; Dong, Y. J.; Dong, C. Z.; Ding, Y. Amorphous CoO_x coupled carbon dots as a spongy porous bifunctional catalyst for efficient photocatalytic water oxidation and CO_2 reduction. *Chin. J. Catal.* **2020**, *41*, 1826–1836.

[6] Sun, W. J.; Lin, J. Q.; Liang, X. M.; Yang, J. Y.; Ma, B. C.; Ding, Y. Recent advances in catalysts based on molecular cubanes for visible light-driven water oxidation. *Acta Phys. Chim. Sin.* **2020**, *36*, 1905025.

[7] Zhang, Y.; Zhu, X. J.; Zhang, G. L.; Shi, P. D.; Wang, A. L. Rational catalyst design for oxygen evolution under acidic conditions: Strategies toward enhanced electrocatalytic performance. *J. Mater. Chem. A* **2021**, *9*, 5890–5914.

[8] Zhang, Y.; Wang, S. X.; Yang, R.; Dai, T. Y.; Zhang, N.; Xi, P. X.; Yan, C. H. Construction of Co_9S_8/MoS_2 heterostructures for enhancing electrocatalytic hydrogen evolution reaction. *Acta Chim. Sin.* **2020**, *78*, 1455–1460.

[9] Joo, J.; Kim, T.; Lee, J.; Choi, S. I.; Lee, K. Morphology-controlled metal sulfides and phosphides for electrochemical water splitting. *Adv. Mater.* **2019**, *31*, 1806682.

[10] Lei, L.; Huang, D. L.; Zhou, C. Y.; Chen, S.; Yan, X. L.; Li, Z. H.; Wang, W. J. Demystifying the active roles of NiFe-based oxides/(oxy)hydroxides for electrochemical water splitting under alkaline conditions. *Coord. Chem. Rev.* **2020**, *408*, 213177.
[11] Zheng, M.; Ding, Y.; Yu, L.; Du, X. Q.; Zhao, Y. K. *In situ* grown pristine cobalt sulfide as bifunctional photocatalyst for hydrogen and oxygen evolution. *Adv. Funct. Mater.* **2017**, *27*, 1605846.
[12] Guo, S. L.; Yuan, H.; Luo, W.; Liu, X. Q.; Zhang, X. T.; Jiang, H. Q.; Liu, F.; Cheng, G. J. Isolated atomic catalysts encapsulated in MOF for ultrafast water pollutant treatment. *Nano Res.* **2021**, *14*, 1287–1293.
[13] Tian, S. B.; Hu, M.; Xu, Q.; Gong, W. B.; Chen, W. X.; Yang, J. R.; Zhu, Y. Q.; Chen, C.; He, J.; Liu, Q. et al. Single-atom Fe with Fe_1N_3 structure showing superior performances for both hydrogenation and transfer hydrogenation of nitrobenzene. *Sci. China Mater.* **2021**, *64*, 642–650.
[14] Li, J.; Li, Y. D.; Zhang, T. Recent progresses in the research of single-atom catalysts. *Sci. China Mater.* **2020**, *63*, 889–891.
[15] Jiang, H. N.; Zhang, P.; Wang, X. G.; Gong, Y. J. Synthesis of magnetic two-dimensional materials by chemical vapor deposition. *Nano Res.* **2021**, *14*, 1789–1801.
[16] Xu, J.; Lai, S. H.; Qi, D. F.; Hu, M.; Peng, X. Y.; Liu, Y. F.; Liu, W.; Hu, G. Z.; Xu, H.; Li, F. et al. Atomic Fe-Zn dual-metal sites for high-efficiency pH-universal oxygen reduction catalysis. *Nano Res.* **2021**, *14*, 1374–1381.
[17] Yang, D. R.; Zuo, S. W.; Yang, H. Z.; Wang, X. Single-unit-cell catalysis of CO_2 electroreduction over sub-1 nm Cu_9S_5 nanowires. *Adv. Energy Mater.* **2021**, *11*, 2100272.
[18] Zhou, M.; Bao, S. J.; Bard, A. J. Probing size and substrate effects on the hydrogen evolution reaction by single isolated Pt atoms, atomic clusters, and nanoparticles. *J. Am. Chem. Soc.* **2019**, *141*, 7327–7332.
[19] Zhang, Q. Q.; Guan, J. Q. Single-atom catalysts for electrocatalytic applications. *Adv. Funct. Mater.* **2020**, *30*, 2000768.
[20] Zhao, D.; Zhuang, Z. W.; Cao, X.; Zhang, C.; Peng, Q.; Chen, C.; Li, Y. D. Atomic site electrocatalysts for water splitting, oxygen reduction and selective oxidation. *Chem. Soc. Rev.* **2020**, *49*, 2215–2264.
[21] Wang, Y.; Mao, J.; Meng, X. G.; Yu, L.; Deng, D. H.; Bao, X. H. Catalysis with two-dimensional materials confining single atoms: Concept, design, and applications. *Chem. Rev.* **2019**, *119*, 1806–1854.
[22] Yang, X. F.; Wang, A. Q.; Qiao, B. T.; Li, J.; Liu, J. Y.; Zhang, T. Single-atom catalysts: A new frontier in heterogeneous catalysis. *Acc. Chem. Res.* **2013**, *46*, 1740–1748.
[23] Ji, S. F.; Chen, Y. J.; Wang, X. L.; Zhang, Z. D.; Wang, D. S.; Li, Y. D. Chemical synthesis of single atomic site catalysts. *Chem. Rev.* **2020**, *120*, 11900–11955.
[24] Song, J. J.; Yang, Y. X.; Liu, S. J.; Li, L.; Yu, N.; Fan, Y. T.; Chen, Z. M.; Kuai, L.; Geng, B. Y. Dispersion and support dictated properties and activities of Pt/metal oxide catalysts in heterogeneous CO oxidation. *Nano Res.*, in press, DOI: 10.1007/s12274-021-3443-7.
[25] Hannagan, R. T.; Giannakakis, G.; Flytzani-Stephanopoulos, M.; Sykes, E. C. H. Single-atom alloy catalysis. *Chem. Rev.* **2020**, *120*, 12044–12088.
[26] He, X. H.; He, Q.; Deng, Y. C.; Peng, M.; Chen, H. Y.; Zhang, Y.; Yao, S. Y.; Zhang, M. T.; Xiao, D. Q.; Ma, D. et al. A versatile route to fabricate single atom catalysts with high chemoselectivity and regioselectivity in hydrogenation. *Nat. Commun.* **2019**, *10*, 3663.
[27] Gao, C.; Low, J.; Long, R.; Kong, T. T.; Zhu, J. F.; Xiong, Y. J. Single-atom photocatalysts: Fundamentals and applications. *Chem. Rev.* **2020**, *120*, 12175–12216.
[28] Sun, T. T.; Xu, L. B.; Wang, D. S.; Li, Y. D. Metal organic frameworks derived single atom catalysts for electrocatalytic energy conversion. *Nano Res.* **2019**, *12*, 2067–2080.
[29] Gong, N. Q.; Ma, X. W.; Ye, X. X.; Zhou, Q. F.; Chen, X. A.; Tan, X. L.; Yao, S. K.; Huo, S. D.; Zhang, T. B.; Chen, S. Z. et al. Carbon-dot-supported atomically dispersed gold as a mitochondrial oxidative stress amplifier for cancer treatment. *Nat. Nanotechnol.* **2019**, *14*, 379–387.
[30] Fei, H. L.; Dong, J. C.; Arellano-Jiménez, M. J.; Ye, G. L.; Kim, N. D.; Samuel, E. L. G.; Peng, Z. W.; Zhu, Z.; Qin, F.; Bao, J. M. et al. Atomic cobalt on nitrogen-doped graphene for hydrogen generation. *Nat. Commun.* **2015**, *6*, 8668.
[31] Fei, H. L.; Dong, J. C.; Feng, Y. X.; Allen, C. S.; Wan, C. Z.; Volosskiy, B.; Li, M. F.; Zhao, Z. P.; Wang, Y. L.; Sun, H. T. et al. General synthesis and definitive structural identification of MN_4C_4 single-atom catalysts with tunable electrocatalytic activities. *Nat. Catal.* **2018**, *1*, 63–72.
[32] Guan, J. Q.; Duan, Z. Y.; Zhang, F. X.; Kelly, S. D.; Si, R.; Dupuis, M.; Huang, Q.; Chen, J. Q.; Tang, C. H.; Li, C. Water oxidation on a mononuclear manganese heterogeneous catalyst. *Nat. Catal.* **2018**, *1*, 870–877.
[33] Fei, H. L.; Dong, J. C.; Chen, D. L.; Hu, T. D.; Duan, X. D.; Shakir, I.; Huang, Y.; Duan, X. F. Single atom electrocatalysts supported on graphene or graphene-like carbons. *Chem. Soc. Rev.* **2019**, *48*, 5207–5241.
[34] Zhang, Q. Q.; Guan, J. Q. Atomically dispersed catalysts for hydrogen/oxygen evolution reactions and overall water splitting. *J. Power Sources* **2020**, *471*, 228446.
[35] Li, J. Z.; Chen, M. J.; Cullen, D. A.; Hwang, S.; Wang, M. Y.; Li, B. Y.; Liu, K. X.; Karakalos, S.; Lucero, M.; Zhang, H. G. et al. Atomically dispersed manganese catalysts for oxygen reduction in proton-exchange membrane fuel cells. *Nat. Catal.* **2018**, *1*, 935–945.
[36] Zhang, Y. K.; Wu, C. Q.; Jiang, H. L.; Lin, Y. X.; Liu, H. J.; He, Q.; Chen, S. M.; Duan, T.; Song, L. Atomic iridium incorporated in cobalt hydroxide for efficient oxygen evolution catalysis in neutral electrolyte. *Adv. Mater.* **2018**, *30*, 1707522.
[37] Cai, C.; Wang, M. Y.; Han, S. B.; Wang, Q.; Zhang, Q.; Zhu, Y. M.; Yang, X. M.; Wu, D. J.; Zu, X. T.; Sterbinsky, G. E. et al. Ultrahigh oxygen evolution reaction activity achieved using Ir single atoms on amorphous CoO_x nanosheets. *ACS Catal.* **2021**, *11*, 123–130.
[38] Wang, Q.; Zhao, Z. L.; Dong, S.; He, D. S.; Lawrence, M. J.; Han, S. B.; Cai, C.; Xiang, S. H.; Rodriguez, P.; Xiang, B. et al. Design of active nickel single-atom decorated MoS_2 as a pH-universal catalyst for hydrogen evolution reaction. *Nano Energy* **2018**, *53*, 458–467.
[39] Zhang, J. M.; Xu, X. P.; Yang, L.; Cheng, D. J.; Cao, D. P. Single-atom Ru doping induced phase transition of MoS_2 and S vacancy for hydrogen evolution reaction. *Small Methods* **2019**, *3*, 1900653.
[40] Meng, X. Y.; Ma, C.; Jiang, L. Z.; Si, R.; Meng, X. G.; Tu, Y. C.; Yu, L.; Bao, X. H.; Deng, D. H. Distance synergy of MoS_2-confined rhodium atoms for highly efficient hydrogen evolution. *Angew. Chem., Int. Ed.* **2020**, *59*, 10502–10507.
[41] Lau, T. H. M.; Lu, X. W.; Kulhavy, J.; Wu, S.; Lu, L. L.; Wu, T. S.; Kato, R.; Foord, J. S.; Soo, Y. L.; Suenaga, K. et al. Transition metal atom doping of the basal plane of MoS_2 monolayer nanosheets for electrochemical hydrogen evolution. *Chem. Sci.* **2018**, *9*, 4769–4776.
[42] Duan, H. L.; Wang, C.; Li, G. N.; Tan, H.; Hu, W.; Cai, L.; Liu, W.; Li, N.; Ji, Q. Q.; Wang, Y. et al. Single-atom-layer catalysis in a MoS_2 monolayer activated by long-range ferromagnetism for the hydrogen evolution reaction: Beyond single-atom catalysis. *Angew. Chem., Int. Ed.* **2021**, *60*, 7251–7258.
[43] Lin, C.; Zhao, Y. H.; Zhang, H. J.; Xie, S. H.; Li, Y. F.; Li, X. P.; Jiang, Z.; Liu, Z. P. Accelerated active phase transformation of NiO powered by Pt single atoms for enhanced oxygen evolution reaction. *Chem. Sci.* **2018**, *9*, 6803–6812.
[44] Liu, D. B.; Ding, S. Q.; Wu, C. Q.; Gan, W.; Wang, C. D.; Cao, D. F.; Rehman, Z. U.; Sang, Y.; Chen, S. M.; Zheng, X. S. et al. Synergistic effect of an atomically dual-metal doped catalyst for highly efficient oxygen evolution. *J. Mater. Chem. A* **2018**, *6*, 6840–6846.
[45] Chung, H. T.; Cullen, D. A.; Higgins, D.; Sneed, B. T.; Holby, E. F.; More, K. L.; Zelenay, P. Direct atomic-level insight into the active sites of a high-performance PGM-free ORR catalyst. *Science* **2017**, *357*, 479–484.
[46] Biesinger, M. C.; Payne, B. P.; Lau, L. W. M.; Gerson, A.; Smart, R. S. C. X-ray photoelectron spectroscopic chemical state quantification of mixed nickel metal, oxide and hydroxide systems. *Surf. Interface Anal.* **2009**, *41*, 324–332.
[47] Qi, K.; Cui, X. Q.; Gu, L.; Yu, S. S.; Fan, X. F.; Luo, M. C.; Xu, S.; Li, N. B.; Zheng, L. R.; Zhang, Q. H. et al. Single-atom cobalt array bound to distorted 1T MoS_2 with ensemble effect for hydrogen evolution catalysis. *Nat. Commun.* **2019**, *10*, 5231.
[48] Li, Y.; Dong, Z.; Jiao, L. F. Multifunctional transition metal-based phosphides in energy-related electrocatalysis. *Adv. Energy Mater.* **2020**, *10*, 1902104.

[49] Wang, J.; Xu, F.; Jin, H. Y.; Chen, Y. Q.; Wang, Y. Non-noble metal-based carbon composites in hydrogen evolution reaction: Fundamentals to applications. *Adv. Mater.* **2017**, *29*, 1605838.
[50] Shi, Y. M.; Zhang, B. Recent advances in transition metal phosphide nanomaterials: Synthesis and applications in hydrogen evolution reaction. *Chem. Soc. Rev.* **2016**, *45*, 1529–1541.
[51] Skúlason, E.; Tripkovic, V.; Björketun, M. E.; Gudmundsdóttir, S.; Karlberg, G.; Rossmeisl, J.; Bligaard, T.; Jónsson, H.; Nørskov, J. K. Modeling the electrochemical hydrogen oxidation and evolution reactions on the basis of density functional theory calculations. *J. Phys. Chem. C* **2010**, *114*, 18182–18197.
[52] Jin, H. Y.; Guo, C. X.; Liu, X.; Liu, J. L.; Vasileff, A.; Jiao, Y.; Zheng, Y.; Qiao, S. Z. Emerging two-dimensional nanomaterials for electrocatalysis. *Chem. Rev.* **2018**, *118*, 6337–6408.
[53] Man, I. C.; Su, H. Y.; Calle-Vallejo, F.; Hansen, H. A.; Martínez, J. I.; Inoglu, N. G.; Kitchin, J.; Jaramillo, T. F.; Norskov, J. K.; Rossmeisl, J. Universality in oxygen evolution electrocatalysis on oxide surfaces. *ChemCatChem* **2011**, *3*, 1159–1165.
[54] Burke, M. S.; Kast, M. G.; Trotochaud, L.; Smith, A. M.; Boettcher, S. W. Cobalt-iron (oxy)hydroxide oxygen evolution electrocatalysts: The role of structure and composition on activity, stability, and mechanism. *J. Am. Chem. Soc.* **2015**, *137*, 3638–3648.
[55] Casalongue, H. G. S.; Ng, M. L.; Kaya, S.; Friebel, D.; Ogasawara, H.; Nilsson, A. *In situ* observation of surface species on iridium oxide nanoparticles during the oxygen evolution reaction. *Angew. Chem., Int. Ed.* **2014**, *53*, 7169–7172.
[56] Pfeifer, V.; Jones, T. E.; Vélez, J. J. V.; Arrigo, R.; Piccinin, S.; Hävecker, M.; Knop-Gericke, A.; Schlögl, R. *In situ* observation of reactive oxygen species forming on oxygen-evolving iridium surfaces. *Chem. Sci.* **2017**, *8*, 2143–2149.
[57] Minguzzi, A.; Lugaresi, O.; Achilli, E.; Locatelli, C.; Vertova, A.; Ghigna, P.; Rondinini, S. Observing the oxidation state turnover in heterogeneous iridium-based water oxidation catalysts. *Chem. Sci.* **2014**, *5*, 3591–3597.
[58] Bai, L. C.; Hsu, C. S.; Alexander, D. T. L.; Chen, H. M.; Hu, X. L. A cobalt-iron double-atom catalyst for the oxygen evolution reaction. *J. Am. Chem. Soc.* **2019**, *141*, 14190–14199.
[59] Zhao, Z. J.; Liu, S. H.; Zha, S. J.; Cheng, D. F.; Studt, F.; Henkelman, G.; Gong, J. L. Theory-guided design of catalytic materials using scaling relationships and reactivity descriptors. *Nat. Rev. Mater.* **2019**, *4*, 792–804.
[60] Seh, Z. W.; Kibsgaard, J.; Dickens, C. F.; Chorkendorff, I.; Nørskov, J. K.; Jaramillo, T. F. Combining theory and experiment in electrocatalysis: Insights into materials design. *Science* **2017**, *355*, eaad4998.
[61] Nørskov, J. K.; Rossmeisl, J.; Logadottir, A.; Lindqvist, L.; Kitchin, J. R.; Bligaard, T.; Jónsson, H. Origin of the overpotential for oxygen reduction at a fuel-cell cathode. *J. Phys. Chem. B* **2004**, *108*, 17886–17892.
[62] Chen, J. Z.; Liu, G. G.; Zhu, Y. Z.; Su, M.; Yin, P. F.; Wu, X. J.; Lu, Q. P.; Tan, C. L.; Zhao, M. T.; Liu, Z. Q. et al. Ag@MoS_2 core-shell heterostructure as SERS platform to reveal the hydrogen evolution active sites of single-layer MoS_2. *J. Am. Chem. Soc.* **2020**, *142*, 7161–7167.
[63] Li, S. S.; Sun, J. R.; Guan, J. Q. Strategies to improve electrocatalytic and photocatalytic performance of two-dimensional materials for hydrogen evolution reaction. *Chin. J. Catal.* **2021**, *42*, 511–556.
[64] Duan, H. L.; Liu, W.; Guo, P.; Tang, F. M.; Yan, W. S.; Yao, T. Identifying the single active site in MoS_2-based hydrogen evolution electrocatalyst by XAFS technique. *Radiat. Phys. Chem.* **2020**, *175*, 108151.
[65] Zhang, H. B.; Yu, L.; Chen, T.; Zhou, W.; Lou, X. W. Surface modulation of hierarchical MoS_2 nanosheets by Ni single atoms for enhanced electrocatalytic hydrogen evolution. *Adv. Funct. Mater.* **2018**, *28*, 1807086.
[66] Hao, Y.; Wang, Y. T.; Xu, L. C.; Yang, Z.; Liu, R. P.; Li, X. Y. 1T-MoS_2 monolayer doped with isolated Ni atoms as highly active hydrogen evolution catalysts: A density functional study. *Appl. Surf. Sci.* **2019**, *469*, 292–297.
[67] Ji, L.; Yan, P. F.; Zhu, C. H.; Ma, C. Y.; Wu, W. Z.; Wei, C.; Shen, Y. L.; Chu, S. Q.; Wang, J. O.; Du, Y. et al. One-pot synthesis of porous 1T-phase MoS_2 integrated with single-atom Cu doping for enhancing electrocatalytic hydrogen evolution reaction. *Appl. Catal. B* **2019**, *251*, 87–93.
[68] Cui, Z. T.; Sa, R. J.; Du, W.; Xiao, C. W.; Li, Q. H.; Ma, Z. J. Theoretical screening of group IIIA-VIIA elements doping to promote hydrogen evolution of MoS_2 basal plane. *Appl. Surf. Sci.* **2021**, *542*, 148535.
[69] Lau, T. H. M.; Wu, S.; Kato, R.; Wu, T. S.; Kulhavý, J.; Mo, J. Y.; Zheng, J. W.; Foord, J. S.; Soo, Y. L.; Suenaga, K. et al. Engineering monolayer 1T-MoS_2 into a bifunctional electrocatalyst via sonochemical doping of isolated transition metal atoms. *ACS Catal.* **2019**, *9*, 7527–7534.
[70] Wu, C. Q.; Li, D. D.; Ding, S. Q.; Rehman, Z. U.; Liu, Q.; Chen, S. M.; Zhang, B.; Song, L. Monoatomic platinum-anchored metallic MoS_2: Correlation between surface dopant and hydrogen evolution. *J. Phys. Chem. Lett.* **2019**, *10*, 6081–6087.
[71] Jiang, K.; Luo, M.; Liu, Z. X.; Peng, M.; Chen, D. C.; Lu, Y. R.; Chan, T. S.; de Groot, F. M. F.; Tan, Y. W. Rational strain engineering of single-atom ruthenium on nanoporous MoS_2 for highly efficient hydrogen evolution. *Nat. Commun.* **2021**, *12*, 1687.
[72] Han, A.; Zhou, X. F.; Wang, X. J.; Liu, S.; Xiong, Q. H.; Zhang, Q. H.; Gu, L.; Zhuang, Z. C.; Zhang, W. J.; Li, F. X. et al. One-step synthesis of single-site vanadium substitution in 1T-WS_2 monolayers for enhanced hydrogen evolution catalysis. *Nat. Commun.* **2021**, *12*, 709.
[73] Yang, Y. J.; Liu, J.; Liu, F.; Wang, Z.; Wu, D. W. FeS_2-anchored transition metal single atoms for highly efficient overall water splitting: A DFT computational screening study. *J. Mater. Chem. A* **2021**, *9*, 2438–2447.
[74] Wang, C. L.; Wu, X.; Zhang, X.; Mu, G.; Li, P. L.; Luo, C.; Xu, H. J.; Di, Z. F. Iron-doped VSe_2 nanosheets for enhanced hydrogen evolution reaction. *Appl. Phys. Lett.* **2020**, *116*, 223901.
[75] Wang, Y. W.; Wan, J.; Tian, W.; Hou, Z. F.; Gu, X.; Wang, Y. Theoretical screening of VSe_2 as support for enhanced electrocatalytic performance of transition-metal single atoms. *J. Colloid Interface Sci.* **2021**, *590*, 210–218.
[76] Liu, Z. L.; Lei, B.; Zhu, Z. L.; Tao, L.; Qi, J.; Bao, D. L.; Wu, X.; Huang, L.; Zhang, Y. Y.; Lin, X. et al. Spontaneous formation of 1D pattern in monolayer VSe_2 with dispersive adsorption of Pt atoms for HER catalysis. *Nano Lett.* **2019**, *19*, 4897–4903.
[77] Shang, H. S.; Zhao, Z. H.; Pei, J. J.; Jiang, Z. L.; Zhou, D. N.; Li, A.; Dong, J. C.; An, P. F.; Zheng, L. R.; Chen, W. X. Dynamic evolution of isolated Ru-FeP atomic interface sites for promoting the electrochemical hydrogen evolution reaction. *J. Mater. Chem. A* **2020**, *8*, 22607–22612.
[78] He, Q.; Tian, D.; Jiang, H. L.; Cao, D. F.; Wei, S. Q.; Liu, D. B.; Song, P.; Lin, Y.; Song, L. Achieving efficient alkaline hydrogen evolution reaction over a Ni_5P_4 catalyst incorporating single-atomic Ru sites. *Adv. Mater.* **2020**, *32*, 1906972.
[79] Zhang, L. H.; Han, L. L.; Liu, H. X.; Liu, X. J.; Luo, J. Potential-cycling synthesis of single platinum atoms for efficient hydrogen evolution in neutral media. *Angew. Chem., Int. Ed.* **2017**, *56*, 13694–13698.
[80] Ye, S. H.; Xiong, W.; Liao, P.; Zheng, L. R.; Ren, X. Z.; He, C. X.; Zhang, Q. L.; Liu, J. H. Removing the barrier to water dissociation on single-atom Pt sites decorated with a CoP mesoporous nanosheet array to achieve improved hydrogen evolution. *J. Mater. Chem. A* **2020**, *8*, 11246–11254.
[81] Wu, J.; Han, N. N.; Ning, S. C.; Chen, T.; Zhu, C. Y.; Pan, C. X.; Wu, H. J.; Pennycook, S. J.; Guan, C. Single-atom tungsten-doped CoP nanoarrays as a high-efficiency pH-universal catalyst for hydrogen evolution reaction. *ACS Sustainable Chem. Eng.* **2020**, *8*, 14825–14832.
[82] Lai, W. H.; Zhang, L. F.; Hua, W. B.; Indris, S.; Yan, Z. C.; Hu, Z.; Zhang, B. W.; Liu, Y. N.; Wang, L.; Liu, M. et al. General π-electron-assisted strategy for Ir, Pt, Ru, Pd, Fe, Ni single-atom electrocatalysts with bifunctional active sites for highly efficient water splitting. *Angew. Chem., Int. Ed.* **2019**, *58*, 11868–11873.
[83] Lv, L.; Yang, Z. X.; Chen, K.; Wang, C. D.; Xiong, Y. J. 2D layered double hydroxides for oxygen evolution reaction: From fundamental design to application. *Adv. Energy Mater.* **2019**, *9*, 1803358.
[84] Li, D.; Chen, X. F.; Lv, Y. Z.; Zhang, G. Y.; Huang, Y.; Liu, W.; Li, Y.; Chen, R. S.; Nuckolls, C.; Ni, H. W. An effective hybrid electrocatalyst for the alkaline HER: Highly dispersed Pt sites

immobilized by a functionalized NiRu-hydroxide. *Appl. Catal. B* **2020**, *269*, 118824.
[85] Gao, J. J.; Du, P.; Zhang, Q. H.; Shen, X.; Chiang, F. K.; Wen, Y. R.; Lin, X.; Liu, X. J.; Qiu, H. J. Platinum single atoms/clusters stabilized in transition metal oxides for enhanced electrocatalysis. *Electrochim. Acta* **2019**, *297*, 155–162.
[86] Zhou, K. L.; Wang, C. C.; Wang, Z. L.; Han, C. B.; Zhang, Q. Q.; Ke, X. X.; Liu, J. B.; Wang, H. Seamlessly conductive $Co(OH)_2$ tailored atomically dispersed Pt electrocatalyst with a hierarchical nanostructure for an efficient hydrogen evolution reaction. *Energy Environ. Sci.* **2020**, *13*, 3082–3092.
[87] Liu, T. T.; Gao, W. B.; Wang, Q. Q.; Dou, M. L.; Zhang, Z. P.; Wang, F. Selective loading of atomic platinum on a $RuCeO_x$ support enables stable hydrogen evolution at high current densities. *Angew. Chem., Int. Ed.* **2020**, *59*, 20423–20427.
[88] Cheng, X.; Lu, Y.; Zheng, L. R.; Cui, Y. T.; Niibe, M.; Tokushima, T.; Li, H. Y.; Zhang, Y. F.; Chen, G.; Sun, S. R. et al. Charge redistribution within platinum-nitrogen coordination structure to boost hydrogen evolution. *Nano Energy* **2020**, *73*, 104739.
[89] Li, M.; Ma, Q.; Zi, W.; Liu, X. J.; Zhu, X. J.; Liu, S. Z. Pt monolayer coating on complex network substrate with high catalytic activity for the hydrogen evolution reaction. *Sci. Adv.* **2015**, *1*, e1400268.
[90] Liao, W. C.; Yau, S. Au(111)-supported Pt monolayer as the most active electrocatalyst toward hydrogen oxidation and evolution reactions in sulfuric acid. *J. Phys. Chem. C* **2017**, *121*, 19218–19225.
[91] Chao, T. T.; Luo, X.; Chen, W. X.; Jiang, B.; Ge, J. J.; Lin, Y.; Wu, G.; Wang, X. Q.; Hu, Y. M.; Zhuang, Z. B. et al. Atomically dispersed copper-platinum dual sites alloyed with palladium nanorings catalyze the hydrogen evolution reaction. *Angew. Chem., Int. Ed.* **2017**, *56*, 16047–16051.
[92] Chen, C. H.; Wu, D. Y.; Li, Z.; Zhang, R.; Kuai, C. G.; Zhao, X. R.; Dong, C. K.; Qiao, S. Z.; Liu, H.; Du, X. W. Ruthenium-based single-atom alloy with high electrocatalytic activity for hydrogen evolution. *Adv. Energy Mater.* **2019**, *9*, 1803913.
[93] Yang, Y.; Xue, X. X.; Chen, Q. J.; Feng, Y. X. Doping single transition metal atom into PtTe sheet for catalyzing nitrogen reduction and hydrogen evolution reactions. *J. Chem. Phys.* **2019**, *151*, 144710.
[94] Li, Y. P.; Chen, S. M.; Long, R.; Ju, H. X.; Wang, Z. W.; Yu, X. X.; Gao, F. Y.; Cai, Z. J.; Wang, C. M.; Xu, Q. et al. Near-surface dilution of trace Pd atoms to facilitate Pd-H bond cleavage for giant enhancement of electrocatalytic hydrogen evolution. *Nano Energy* **2017**, *34*, 306–312.
[95] Feng, Y. Y.; Guan, Y. X.; Zhang, H. J.; Huang, Z. Y.; Li, J.; Jiang, Z. Q.; Gu, X.; Wang, Y. Selectively anchoring Pt single atoms at hetero-interfaces of γ-Al_2O_3/NiS to promote the hydrogen evolution reaction. *J. Mater. Chem. A* **2018**, *6*, 11783–11789.
[96] Wang, L. G.; Duan, X. X.; Liu, X. J.; Gu, J.; Si, R.; Qiu, Y.; Qiu, Y. M.; Shi, D. E.; Chen, F. H.; Sun, X. M. et al. Atomically dispersed Mo supported on metallic Co_9S_8 nanoflakes as an advanced noble-metal-free bifunctional water splitting catalyst working in universal pH conditions. *Adv. Energy Mater.* **2020**, *10*, 1903137.
[97] Dai, J.; Zhu, Y. L.; Tahini, H. A.; Lin, Q.; Chen, Y.; Guan, D. Q.; Zhou, C.; Hu, Z. W.; Lin, H. J.; Chan, T. S. et al. Single-phase perovskite oxide with super-exchange induced atomic-scale synergistic active centers enables ultrafast hydrogen evolution. *Nat. Commun.* **2020**, *11*, 5657.
[98] Xu, H. T.; Liu, T. Y.; Bai, S. X.; Li, L. G.; Zhu, Y. M.; Wang, J.; Yang, S. Z.; Li, Y. F.; Shao, Q.; Huang, X. Q. Cation exchange strategy to single-atom noble-metal doped CuO nanowire arrays with ultralow overpotential for H_2O splitting. *Nano Lett.* **2020**, *20*, 5482–5489.
[99] Jiang, K.; Liu, B. Y.; Luo, M.; Ning, S. C.; Peng, M.; Zhao, Y.; Lu, Y. R.; Chan, T. S.; de Groot, F. M. F.; Tan, Y. W. Single platinum atoms embedded in nanoporous cobalt selenide as electrocatalyst for accelerating hydrogen evolution reaction. *Nat. Commun.* **2019**, *10*, 1743.
[100] Babu, D. D.; Huang, Y. Y.; Anandhababu, G.; Wang, X.; Si, R.; Wu, M. X.; Li, Q. H.; Wang, Y. B.; Yao, J. N. Atomic iridium@cobalt nanosheets for dinuclear tandem water oxidation. *J. Mater. Chem. A* **2019**, *7*, 8376–8383.
[101] Pearson, R. G. Absolute electronegativity and hardness: Application to inorganic chemistry. *Inorg. Chem.* **1988**, *27*, 734–740.
[102] Xing, Y. L.; Ku, J. G.; Fu, W.; Wang, L. Z.; Chen, H. H. Inductive effect between atomically dispersed iridium and transition-metal hydroxide nanosheets enables highly efficient oxygen evolution reaction. *Chem. Eng. J.* **2020**, *395*, 125149.
[103] Yin, J.; Jin, J.; Lu, M.; Huang, B. L.; Zhang, H.; Peng, Y.; Xi, P. X.; Yan, C. H. Iridium single atoms coupling with oxygen vacancies boosts oxygen evolution reaction in acid media. *J. Am. Chem. Soc.* **2020**, *142*, 18378–18386.
[104] Zhou, Y. C.; López, N. The role of Fe species on NiOOH in oxygen evolution reactions. *ACS Catal.* **2020**, *10*, 6254–6261.
[105] Zhang, S.; Huang, B. L.; Wang, L. G.; Zhang, X. Y.; Zhu, H. S.; Zhu, X. Q.; Li, J.; Guo, S. J.; Wang, E. K. Boosted oxygen evolution reactivity via atomic iron doping in cobalt carbonate hydroxide hydrate. *ACS Appl. Mater. Interfaces* **2020**, *12*, 40220–40228.
[106] Friebel, D.; Louie, M. W.; Bajdich, M.; Sanwald, K. E.; Cai, Y.; Wise, A. M.; Cheng, M. J.; Sokaras, D.; Weng, T. C.; Alonso-Mori, R. et al. Identification of highly active fe sites in (Ni,Fe)OOH for electrocatalytic water splitting. *J. Am. Chem. Soc.* **2015**, *137*, 1305–1313.
[107] Chen, J. Y. C.; Dang, L. N.; Liang, H. F.; Bi, W. L.; Gerken, J. B.; Jin, S.; Alp, E. E.; Stahl, S. S. *Operando* analysis of NiFe and Fe oxyhydroxide electrocatalysts for water oxidation: Detection of Fe^{4+} by Mossbauer spectroscopy. *J. Am. Chem. Soc.* **2015**, *137*, 15090–15093.
[108] Zhu, K. Y.; Zhu, X. F.; Yang, W. S. Application of *in situ* techniques for the characterization of NiFe-based oxygen evolution reaction (OER) electrocatalysts. *Angew. Chem., Int. Ed.* **2019**, *58*, 1252–1265.
[109] Hu, Y. D.; Luo, G.; Wang, L. G.; Liu, X. K.; Qu, Y. T.; Zhou, Y. S.; Zhou, F. Y.; Li, Z. J.; Li, Y. F.; Yao, T. et al. Single Ru atoms stabilized by hybrid amorphous/crystalline FeCoNi layered double hydroxide for ultraefficient oxygen evolution. *Adv. Energy Mater.* **2021**, *11*, 2002816.
[110] Li, P. S.; Wang, M. Y.; Duan, X. X.; Zheng, L. R.; Cheng, X. P.; Zhang, Y. F.; Kuang, Y.; Li, Y. P.; Ma, Q.; Feng, Z. X. et al. Boosting oxygen evolution of single-atomic ruthenium through electronic coupling with cobalt-iron layered double hydroxides. *Nat. Commun.* **2019**, *10*, 1711.
[111] Dong, C. L.; Zhang, X. L.; Xu, J.; Si, R.; Sheng, J.; Luo, J.; Zhang, S. N.; Dong, W. J.; Li, G. B.; Wang, W. C. et al. Ruthenium-doped cobalt-chromium layered double hydroxides for enhancing oxygen evolution through regulating charge transfer. *Small* **2020**, *16*, 1905328.
[112] Baeumer, C.; Li, J.; Lu, Q. Y.; Liang, A. Y. L.; Jin, L.; Martins, H. P.; Duchoň, T.; Glöß, M.; Gericke, S. M.; Wohlgemuth, M. A. et al. Tuning electrochemically driven surface transformation in atomically flat $LaNiO_3$ thin films for enhanced water electrolysis. *Nat. Mater.* **2021**, *20*, 674–682.
[113] Harzandi, A. M.; Shadman, S.; Nissimagoudar, A. S.; Kim, D. Y.; Lim, H. D.; Lee, J. H.; Kim, M. G.; Jeong, H. Y.; Kim, Y.; Kim, K. S. Ruthenium core-shell engineering with nickel single atoms for selective oxygen evolution via nondestructive mechanism. *Adv. Energy Mater.* **2021**, *11*, 2003448.
[114] Guan, J. Q.; Ding, C. M.; Chen, R. T.; Huang, B. K.; Zhang, X. W.; Fan, F. T.; Zhang, F. X.; Li, C. CoO_x nanoparticle anchored on sulfonated-graphite as efficient water oxidation catalyst. *Chem. Sci.* **2017**, *8*, 6111–6116.
[115] Liu, C.; Qian, J.; Ye, Y. F.; Zhou, H.; Sun, C. J.; Sheehan, C.; Zhang, Z. Y.; Wan, G.; Liu, Y. S.; Guo, J. H. et al. Oxygen evolution reaction over catalytic single-site Co in a well-defined brookite TiO_2 nanorod surface. *Nat. Catal.* **2021**, *4*, 36–45.
[116] Jiang, K.; Luo, M.; Peng, M.; Yu, Y. Q.; Lu, Y. R.; Chan, T. S.; Liu, P.; de Groot, F. M. F.; Tan, Y. W. Dynamic active-site generation of atomic iridium stabilized on nanoporous metal phosphides for water oxidation. *Nat. Commun.* **2020**, *11*, 2701.
[117] Cai, C.; Han, S. B.; Wang, Q.; Gu, M. Direct observation of yolk-shell transforming to gold single atoms and clusters with superior oxygen evolution reaction efficiency. *ACS Nano* **2019**, *13*, 8865–8871.
[118] He, F.; Liu, Y. J.; Cai, Q. H.; Zhao, J. X. Size-dependent electrocatalytic activity of ORR/OER on palladium nanoclusters anchored on defective MoS_2 monolayers. *New J. Chem.* **2020**, *44*, 16135–16143.
[119] Wohlfahrt-Mehrens, M.; Heitbaum, J. Oxygen evolution on Ru and

RuO_2 electrodes studied using isotope labelling and on-line mass spectrometry. *J. Electroanal. Chem. Interfacial Electrochem.* **1987**, *237*, 251–260.

[120] Binninger, T.; Mohamed, R.; Waltar, K.; Fabbri, E.; Levecque, P.; Kötz, R.; Schmidt, T. J. Thermodynamic explanation of the universal correlation between oxygen evolution activity and corrosion of oxide catalysts. *Sci. Rep.* **2015**, *5*, 12167.

[121] Grimaud, A.; Díaz-Morales, O.; Han, B. H.; Hong, W. T.; Lee, Y. L.; Giordano, L.; Stoerzinger, K. A.; Koper, M. T. M.; Shao-Horn, Y. Activating lattice oxygen redox reactions in metal oxides to catalyse oxygen evolution. *Nat. Chem.* **2017**, *9*, 457–465.

[122] Bai, L.; Duan, Z. Y.; Wen, X. D.; Si, R.; Zhang, Q. Q.; Guan, J. Q. Highly dispersed ruthenium-based multifunctional electrocatalyst. *ACS Catal.* **2019**, *9*, 9897–9904.

[123] Yao, Y. C.; Hu, S. L.; Chen, W. X.; Huang, Z. Q.; Wei, W. C.; Yao, T.; Liu, R. R.; Zang, K. T.; Wang, X. Q.; Wu, G. et al. Engineering the electronic structure of single atom Ru sites via compressive strain boosts acidic water oxidation electrocatalysis. *Nat. Catal.* **2019**, *2*, 304–313.

[124] Mannix, A. J.; Zhou, X. F.; Kiraly, B.; Wood, J. D.; Alducin, D.; Myers, B. D.; Liu, X. L.; Fisher, B. L.; Santiago, U.; Guest, J. R. et al. Synthesis of borophenes: Anisotropic, two-dimensional boron polymorphs. *Science* **2015**, *350*, 1513–1516.

[125] Feng, B. J.; Zhang, J.; Zhong, Q.; Li, W. B.; Li, S.; Li, H.; Cheng, P.; Meng, S.; Chen, L.; Wu, K. H. Experimental realization of two-dimensional boron sheets. *Nat. Chem.* **2016**, *8*, 563–568.

[126] Wu, R. Y.; Drozdov, I. K.; Eltinge, S.; Zahl, P.; Ismail-Beigi, S.; Božović, I.; Gozar, A. Large-area single-crystal sheets of borophene on Cu(111) surfaces. *Nat. Nanotechnol.* **2019**, *14*, 44–49.

[127] Kiraly, B.; Liu, X. L.; Wang, L. Q.; Zhang, Z. H.; Mannix, A. J.; Fisher, B. L.; Yakobson, B. I.; Hersam, M. C.; Guisinger, N. P. Borophene synthesis on Au(111). *ACS Nano* **2019**, *13*, 3816–3822.

[128] Banerjee, A.; Chakraborty, S.; Jena, N. K.; Ahuja, R. Scrupulous probing of bifunctional catalytic activity of borophene monolayer: Mapping reaction coordinate with charge transfer. *ACS Appl. Energy Mater.* **2018**, *1*, 3571–3576.

[129] Mohajeri, A.; Dashti, N. L. Cooperativity in bimetallic SACs: An efficient strategy for designing bifunctional catalysts for overall water splitting. *J. Phys. Chem. C* **2019**, *123*, 30972–30980.

[130] Singh, Y.; Back, S.; Jung, Y. Computational exploration of borophane-supported single transition metal atoms as potential oxygen reduction and evolution electrocatalysts. *Phys. Chem. Chem. Phys.* **2018**, *20*, 21095–21104.

[131] Xu, X. W.; Si, R. H.; Dong, Y.; Li, L. L.; Zhang, M. H.; Wu, X. Y.; Zhang, J.; Fu, K.; Guo, Y.; He, Y. Y. Borophene-supported single transition metal atoms as potential oxygen evolution/reduction electrocatalysts: A density functional theory study. *J. Mol. Model.* **2021**, *27*, 67.

[132] Zeng, H. H.; Liu, X. Y.; Chen, F. B.; Chen, Z. G.; Fan, X. L.; Lau, W. Single atoms on a nitrogen-doped boron phosphide monolayer: A new promising bifunctional electrocatalyst for ORR and OER. *ACS Appl. Mater. Interfaces* **2020**, *12*, 52549–52559.

[133] Liu, N.; Duan, Z. Y.; Zhang, Q. Q.; Guan, J. Q. Insights into active species of ultrafine iridium oxide nanoparticle electrocatalysts in hydrogen/oxygen evolution reactions. *Chem. Eng. J.* **2021**, *419*, 129567.

[134] Ling, C. Y.; Shi, L.; Ouyang, Y. X.; Zeng, X. C.; Wang, J. L. Nanosheet supported single-metal atom bifunctional catalyst for overall water splitting. *Nano Lett.* **2017**, *17*, 5133–5139.

[135] Xu, X. P.; Xu, H. X.; Cheng, D. J. Design of high-performance MoS_2 edge supported single-metal atom bifunctional catalysts for overall water splitting via a simple equation. *Nanoscale* **2019**, *11*, 20228–20237.

[136] Hwang, J.; Noh, S. H.; Han, B. Design of active bifunctional electrocatalysts using single atom doped transition metal dichalcogenides. *Appl. Surf. Sci.* **2019**, *471*, 545–552.

[137] Wang, Y.; Zheng, P.; Li, M. X.; Li, Y. R.; Zhang, X.; Chen, J.; Fang, X.; Liu, Y. J.; Yuan, X. L.; Dai, X. P. et al. Interfacial synergy between dispersed Ru sub-nanoclusters and porous NiFe layered double hydroxide on accelerated overall water splitting by intermediate modulation. *Nanoscale* **2020**, *12*, 9669–9679.

[138] Xiong, D. H.; Zhang, Q. Q.; Li, W.; Li, J. J.; Fu, X. L.; Cerqueira, M. F.; Alpuim, P.; Liu, L. F. Atomic-layer-deposited ultrafine MoS_2 nanocrystals on cobalt foam for efficient and stable electrochemical oxygen evolution. *Nanoscale* **2017**, *9*, 2711–2717.

[139] Wang, Q.; Huang, X.; Zhao, Z. L.; Wang, M. Y.; Xiang, B.; Li, J.; Feng, Z. X.; Xu, H.; Gu, M. Ultrahigh-loading of Ir single atoms on NiO matrix to dramatically enhance oxygen evolution reaction. *J. Am. Chem. Soc.* **2020**, *142*, 7425–7433.

[140] Zhang, X. P.; Dong, C. L.; Wang, Y. Q.; Chen, J.; Arul, K. T.; Diao, Z. D.; Fu, Y. M.; Li, M. T.; Shen, S. H. Regulating crystal structure and atomic arrangement in single-component metal oxides through electrochemical conversion for efficient overall water splitting. *ACS Appl. Mater. Interfaces* **2020**, *12*, 57038–57046.

[141] Peng, X. Y.; Zhao, S. Z.; Mi, Y. Y.; Han, L. L.; Liu, X. J.; Qi, D. F.; Sun, J. Q.; Liu, Y. F.; Bao, H. H.; Zhuo, L. C. et al. Trifunctional single-atomic Ru sites enable efficient overall water splitting and oxygen reduction in acidic media. *Small* **2020**, *16*, 2002888.